Cell Systems

NAD+ flux is maintained in aged mice despite lower tissue concentrations

Graphical abstract

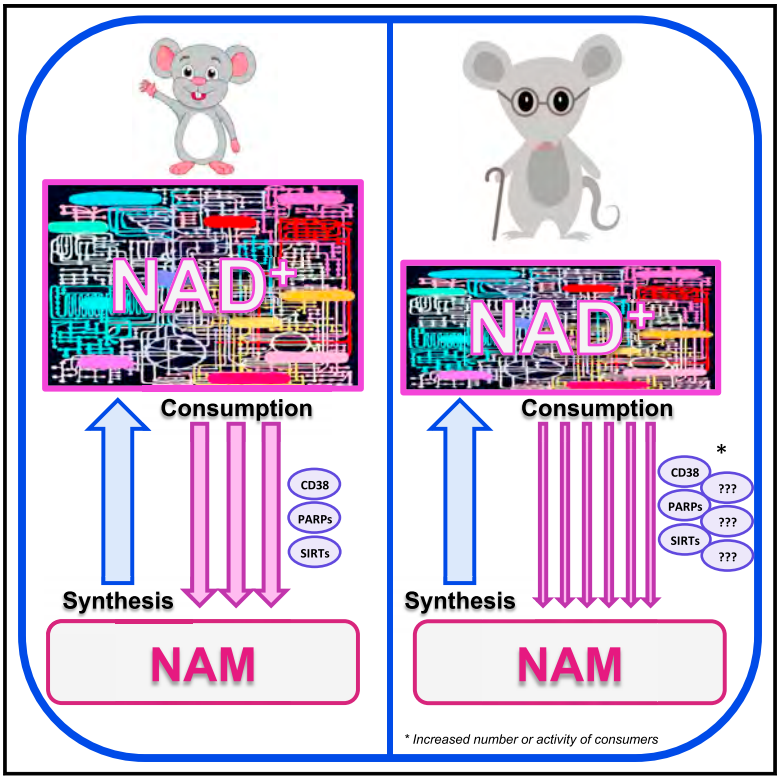

Highlights

- NAD+ pool size decreased in aged tissues without a change in circulating precursors
- Whole-body synthesis of NAD+ is not impaired in aged mice
- Maintained NAD+ turnover despite lower concentration indicates higher consumer activity
- Acute inflammatory stress impairs NAD+ synthesis

Authors

Melanie R. McReynolds, Karthikeyani Chellappa, Eric Chiles, ..., Xiaoyang Su, Joshua D. Rabinowitz, Joseph A. Baur

Correspondence

joshr@princeton.edu (J.D.R.), baur@pennmedicine.upenn.edu (J.A.B.)

In brief

NAD+ is an essential redox cofactor and a substrate for signaling enzymes that influence many aspects of cellular physiology. NAD+ concentration falls with age in some tissues, which has been attributed to decreased synthesis or increased consumption. Here, we provide the first direct measurements of changes in NAD+ turnover flux with age, finding that synthesis is maintained despite the lower NAD+ concentrations in many aged tissues. We further characterize the effects of caloric restriction and inflammatory stress on NAD+ turnover.

McReynolds et al., 2021, Cell Systems *12*, 1–13
December 15, 2021
https://doi.org/10.1016/j.cels.2021.09.001

Please cite this article in press as: McReynolds et al., NAD+ flux is maintained in aged mice despite lower tissue concentrations, Cell Systems (2021), https://doi.org/10.1016/j.cels.2021.09.001

Cell Systems

CellPress

Article

NAD+ flux is maintained in aged mice despite lower tissue concentrations

Melanie R. McReynolds,[1,2,8] Karthikeyani Chellappa,[3,8] Eric Chiles,[4] Connor Jankowski,[1] Yihui Shen,[1,2] Li Chen,[1,2] Hélène C. Descamps,[5] Sarmistha Mukherjee,[3] Yashaswini R. Bhat,[3] Siddharth R. Lingala,[3] Qingwei Chu,[3] Paul Botolin,[3] Faisal Hayat,[6] Tomohito Doke,[7] Katalin Susztak,[7] Christoph A. Thaiss,[5] Wenyun Lu,[1,2] Marie E. Migaud,[6] Xiaoyang Su,[4] Joshua D. Rabinowitz,[1,2,*] and Joseph A. Baur[3,9,*]

[1]Lewis-Sigler Institute for Integrative Genomics, Princeton University, Princeton, NJ, USA
[2]Department of Chemistry, Princeton University, Princeton, NJ, USA
[3]Department of Physiology and Institute for Diabetes, Obesity, and Metabolism, Perelman School of Medicine, University of Pennsylvania, Philadelphia, PA, USA
[4]Department of Medicine, Robert Wood Johnson Medical School, Rutgers University, New Brunswick, NJ, USA
[5]Department of Microbiology, Perelman School of Medicine, University of Pennsylvania, Philadelphia, PA, USA
[6]Department of Pharmacology, Mitchell Cancer Institute, College of Medicine, University of South Alabama, Mobile, AL, USA
[7]Department of Medicine, Renal Electrolyte and Hypertension Division, University of Pennsylvania, Philadelphia, PA, USA
[8]These authors contributed equally
[9]Lead contact
*Correspondence: joshr@princeton.edu (J.D.R.), baur@pennmedicine.upenn.edu (J.A.B.)
https://doi.org/10.1016/j.cels.2021.09.001

SUMMARY

NAD+ is an essential coenzyme for all living cells. NAD+ concentrations decline with age, but whether this reflects impaired production or accelerated consumption remains unclear. We employed isotope tracing and mass spectrometry to probe age-related changes in NAD+ metabolism across tissues. In aged mice, we observed modest tissue NAD+ depletion (median decrease ~30%). Circulating NAD+ precursors were not significantly changed, and isotope tracing showed the unimpaired synthesis of nicotinamide from tryptophan. In most tissues of aged mice, turnover of the smaller tissue NAD+ pool was modestly faster such that absolute NAD+ biosynthetic flux was maintained, consistent with more active NAD+-consuming enzymes. Calorie restriction partially mitigated age-associated NAD+ decline by decreasing consumption. Acute inflammatory stress induced by LPS decreased NAD+ by impairing synthesis in both young and aged mice. Thus, the decline in NAD+ with normal aging is relatively subtle and occurs despite maintained NAD+ production, likely due to increased consumption.

INTRODUCTION

Aging is the strongest risk factor for the most prevalent diseases in developed nations, including diabetes, cancer, cardiovascular, and neurodegenerative disorders. Demographics are projected to continue to shift toward a higher proportion of aged individuals, making it imperative to identify strategies to promote healthier aging. Nicotinamide adenine dinucleotide (NAD^+) is an essential coenzyme in redox reactions and co-substrate for signaling enzymes (Pollak et al., 2007; Srivastava, 2016; Yang and Sauve, 2016). NAD^+ concentration decreases with age in worms, flies, mice, and humans (Chini et al., 2017; Gomes et al., 2013; McReynolds et al., 2020; Mouchiroud et al., 2013; Yoshino et al., 2018; Zhang et al., 2016). NAD^+ depletion causes multiple defects including mitochondrial dysfunction, deregulated nutrient sensing, and epigenetic alterations (Gomes et al., 2013; Salvatori et al., 2017; Verdin, 2015). NAD^+ pools can be safely supplemented by oral precursors, and such supplementation has been reported to have beneficial effects in aged mice (Mills et al., 2016; Mitchell et al., 2018; Zhang et al., 2016). Thus, decreased NAD^+ availability may be a contributing and modifiable factor in age-related diseases. The mechanisms controlling its levels in aging, however, remain incompletely understood.

NAD^+ is best known for its role as an oxidoreductase cofactor. By accepting and donating hydride ions (H^-), NAD^+ plays a central role in metabolism, supporting myriad biochemical reactions including of glycolysis, oxidative phosphorylation, and β-oxidation (Pollak et al., 2007). NAD^+ also serves as a co-substrate for signaling enzymes, including the sirtuins (SIRTs), poly ADP-ribosyl polymerases (PARPs), cyclic ADP-ribose synthases (CD38/CD157), mono-ADP-ribosyltransferases, and Sterile Alpha and Toll/interleukin-1 Receptor Motif-Containing 1 (SARM1). These enzymes continuously degrade intracellular NAD^+ and release nicotinamide (NAM), necessitating a means to replenish the NAD^+ pool (McReynolds et al., 2020). In mammals, NAD^+ is made *de novo* from tryptophan and via the Preiss-Handler pathway from nicotinic acid, but the bulk of

Please cite this article in press as: McReynolds et al., NAD+ flux is maintained in aged mice despite lower tissue concentrations, Cell Systems (2021), https://doi.org/10.1016/j.cels.2021.09.001

synthesis in most tissues occurs via the salvage pathway from nicotinamide (NAM) (Liu et al., 2018) (Figure S1A). Thus, the balance between NAD^+ consumption and synthesis from NAM likely determines the steady-state concentration in most tissues.

A decrease in NAD^+ concentration with age could be driven by either an increase in consumer activity or a decrease in synthesis. Increased PARP activity, potentially as a direct result of increased DNA damage, could drive age-related NAD^+ decline, and inhibition of PARPs is sufficient to block NAD^+ depletion and premature aging in a mouse model with defective DNA repair (Bai et al., 2011; Fang et al., 2014; Scheibye-Knudsen et al., 2014; Wang et al., 2014). Other data support CD38 being a primary cause of age-related NAD^+ decline. CD38 is expressed primarily by immune and endothelial cells and increased immune cell infiltration and CD38 expression and activity are observed in aged tissues (Tarragó et al., 2018). This is due at least in part to the recruitment of CD38-positive cells by senescent cells within aged tissues (Chini et al., 2020; Covarrubias et al., 2020). Moreover, CD38 knockout mice have elevated NAD^+ that persists into older age (Tarragó et al., 2018). These observations support increased consumer activity as the driver of age-related NAD^+ decline via inflammation (CD38) (Amici et al., 2018; Camacho-Pereira et al., 2016; Chini et al., 2019; Kang et al., 2006; Matalonga et al., 2017; Musso et al., 2001) or DNA damage (PARP1) (Massudi et al., 2012; Scheibye-Knudsen et al., 2014; Ubaida-Mohien et al., 2019). On the other hand, mRNA and protein expression of nicotinamide phosphoribosyltransferase (NAMPT), the rate-limiting enzyme in the NAD^+ salvage pathway, is reduced with age in multiple tissues (Mills et al., 2016; Stein and Imai, 2014), as is its extracellular form in the circulation (Yoshida et al., 2019). Similarly, expression levels of nicotinamide mononucleotide adenylyl transferase (NMNAT) isoforms are reduced in liver, kidney, oocytes, and colon of aged mice (Camacho-Pereira et al., 2016; Guan et al., 2017; Wu et al., 2019; Zhu et al., 2017). These observations suggest the alternative hypothesis that NAD^+ decline could be driven by decreased synthesis. At present, it remains unclear whether consumption or synthesis is the primary driver of age-related decline in NAD^+ availability. Differentiating these possibilities may allow more targeted therapeutic strategies to restore or boost NAD^+ levels. However, steady-state concentration measurements are ill-suited to this task. Thus, there is a need to examine NAD^+ metabolic flux, i.e., the rates of production and degradation of the NAD^+ chemical backbone in aged tissues.

To this end, we employed isotope-labeled NAD^+ precursors, mass spectrometry, and quantitative modeling to determine NAD^+ fluxes in young and aged mice. We first quantified the NAD^+ metabolome across twenty-one tissues, finding that NAD^+ pools are reduced modestly with age in certain tissues. Then, using isotope tracers, we show that NAD^+ synthesis is maintained with age, pointing to increased consumer activity as the primary driver of age-related NAD^+ decline.

RESULTS

NAD^+ metabolism is altered with age

We measured the steady-state NAD^+ metabolome in tissues of young (3 months) and aged (25 months) C57BL/6 mice from the National Institute of Aging (NIA)'s aged rodent colony (Figure 1A). NAD^+ and $NADP^+$ modestly declined with age in most tissues, with the degree of change highly tissue dependent (Figures 1B–1E). NAD^+ pools significantly decreased in aged mice in the liver, kidney, intestine, skeletal muscle, and adipose (Figures 1B and S1B). Reduced forms of each nucleotide, NADH and NADPH, did not decrease consistently with age, declining significantly only in the liver and increasing in the brain (Figures 1C, 1E, S1C, and S1D).

We next examined the ratio of oxidized to reduced NAD(H) and NADP(H) in each tissue with age. A more reduced NAD(H) redox state with age has previously been reported for multiple tissues in rats (Braidy et al., 2011), human brains (Zhu et al., 2015), and human plasma (Clement et al., 2019), and we observed a similar pattern in mouse (Figure 1F), with the notable exception of liver, which exhibited a significantly more oxidized redox state with age (Figures 1F and 1G).

These changes in NAD(H) and NADP(H) levels in aged mice occurred without any consistent change in circulating NAM, the major NAD^+ precursor for most tissues (Figure S1E). In addition, there was no alteration in circulating levels of methylated NAM, the primary catabolic product of nicotinamide, which is eventually oxidized and excreted in the urine (Figure S1F). Circulating NR levels were also unchanged with age (Figure S1G) (NMN was not consistently detected in serum samples using our methodology). Changes in tissue levels of NAD^+-related metabolites were modest, with the exception of increased kynurenine in the brain (Figure S1H). Thus, aging decreases the concentration of NAD^+ without major changes in the abundance of circulating precursors.

Flux from tryptophan to circulating NAM is not altered with age

The liver converts dietary tryptophan to NAD^+ via the *de novo* pathway and releases NAM, which serves as a precursor for NAD^+ synthesis in other tissues (Liu et al., 2018). Kynurenine is an intermediate in the *de novo* pathway that can influence the immune and nervous systems. Circulating Trp and kynurenine levels were not altered with age (Figures 2A and 2B). However, only a small proportion of Trp is used for NAD^+ synthesis (Shibata, 2018), meaning that substantial changes in *de novo* NAD^+ flux might be hard to detect at the level of Trp concentration. To test whether *de novo* NAD^+ synthesis from tryptophan was deranged with age, we employed isotope tracing. [U-^{13}C] Trp (M+11) was infused at a constant rate of 2.5 nmol/g/min for 15 h, achieving serum enrichment of ~60% (M+11) tryptophan in both young and aged mice (Figures 2C and 2D). This was mirrored by similar enrichment (M+10) in the kynurenine pool (Figure 2E), and the eventual appearance of the downstream metabolites 3-hydroxyanthranilic acid (3HAA, M+6) and NAM (M+6) (Figures 2F and 2G). In all cases, the labeling patterns were indistinguishable between old and young animals. Experiments infusing [U-^{13}C]Trp (M+11) orally also showed no age effect (Figures S2A–S2L). Labeled NAM (M+6) and NAD^+ (M+6) from tryptophan were highly enriched in the liver, which is the major site of *de novo* synthesis (Figures 2H and 2I). The fractional labeling of NAM in other tissues was below that in the circulation, suggesting that it could be explained entirely by uptake of labeled NAM (Figure 2H). However, we cannot exclude the possibility that low levels of *de novo* synthesis were also present in

Please cite this article in press as: McReynolds et al., NAD+ flux is maintained in aged mice despite lower tissue concentrations, Cell Systems (2021), https://doi.org/10.1016/j.cels.2021.09.001

CellPress

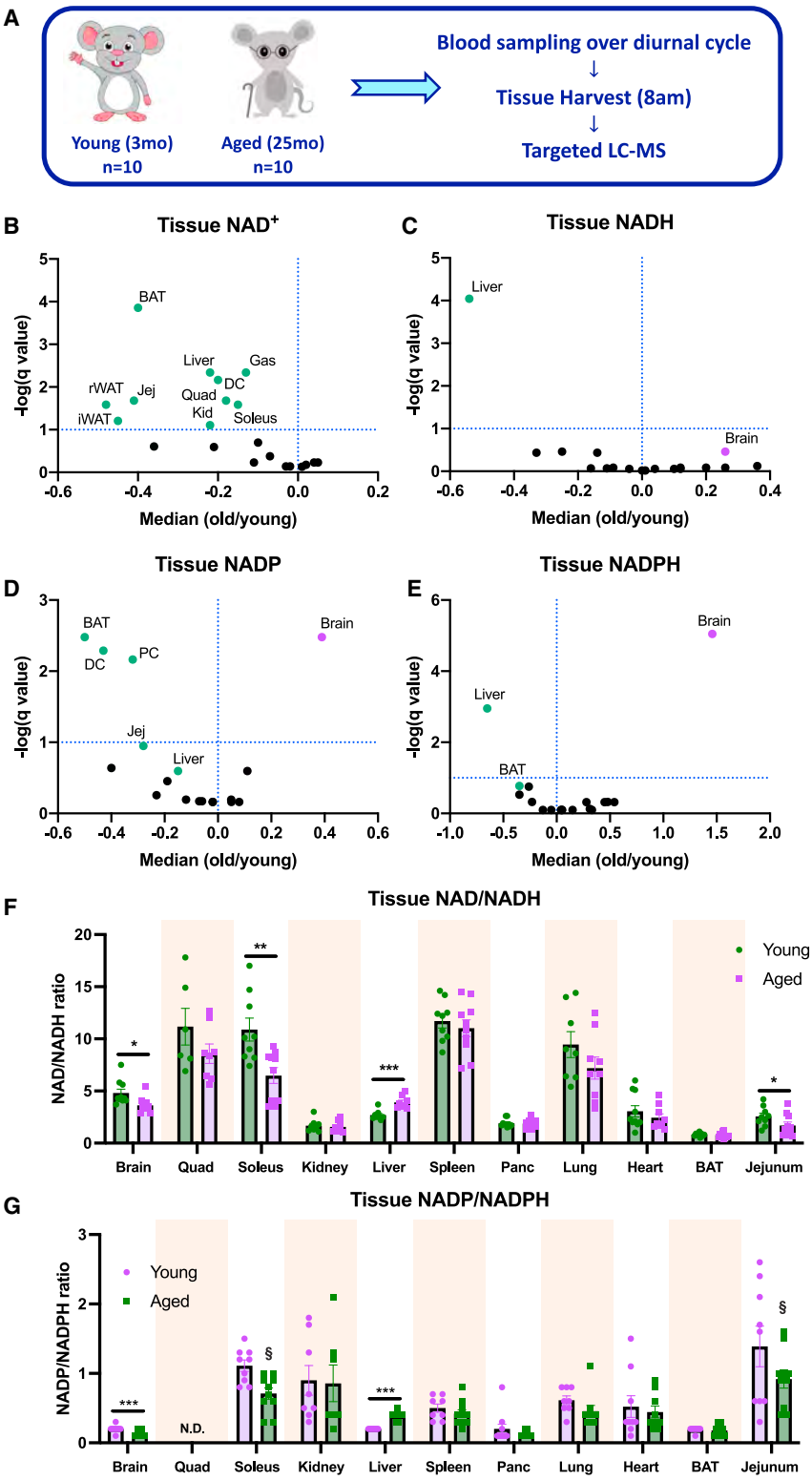

Figure 1. NAD+ metabolism is altered with age

(A) Schematic for collecting serum and tissue harvesting in young (3mo) and aged (25mo) C57BL/6 mice from NIA aged colony.

(B–E) Volcano plot representing LC-MS measurements for NAD(H) and NADP(H) across tissues in aged versus young mice. The x axis represents the median and the y axis represents adjusted FDR. Dotted lines represent FDR q < 0.1 calculated by Banjamiini, Krieger, and Yekutieli multiple comparison test, and colored dots indicated tissues that change with age significantly, calculated by Student's t test.

(F and G) Redox ratio alterations with age in liver, brain, and jejunum. For all panels, *error bars* indicate SEM ***p < 0.001; **p < 0.01; *p < 0.05; §p < 0.1, calculated with Student's t test.

Please cite this article in press as: McReynolds et al., NAD+ flux is maintained in aged mice despite lower tissue concentrations, Cell Systems (2021), https://doi.org/10.1016/j.cels.2021.09.001

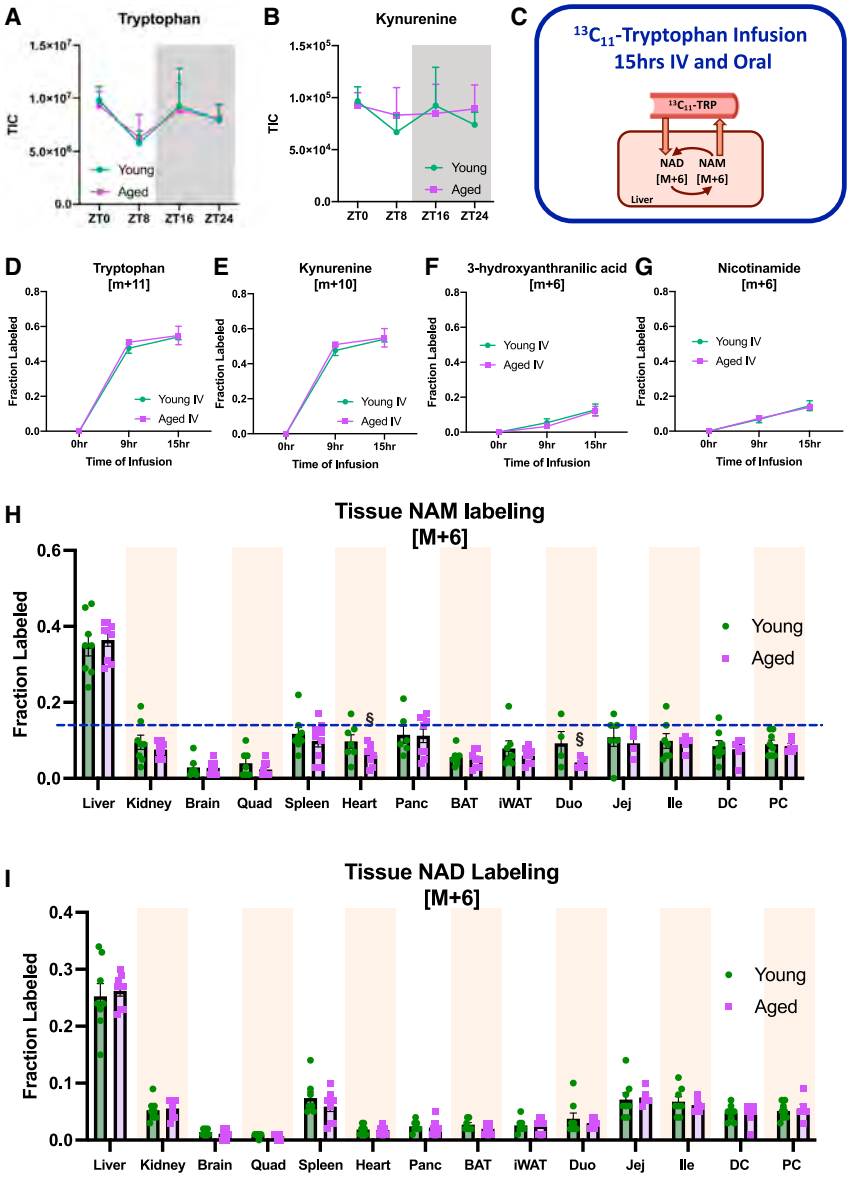

Figure 2. Flux from tryptophan to circulating NAM is not altered with age

(A and B) LC-MS measurements of Trp metabolites (Trp and Kyn) in circulation.

(C) Experimental design for infusing universally labeled-Trp intravenously and orally in young (3mo) and aged (25mo) C57BL/6 mice.

(D) Fraction Trp labeling over 15 h.

(E) Fraction Kyn labeling.

(F) Fraction 3HAA labeling.

(G) Fraction NAM labeling from Trp in young and aged mice circulation.

(H) Tissue NAM labeling from Trp. Dashed line represents serum NAM enrichment highlighting that the liver exceeds serum NAM labeling and all other tissues fall below serum enrichment.

(I) Tissue NAD^+ labeling from Trp. Tissue labeling combines both oral and IV infusion due to nearly identical labeling patterns. Young, n = 7–8; aged, n = 6–9. For all panels, error bars indicate SEM ***p < 0.001; **p < 0.01; *p < 0.05; §p < 0.1, calculated with Student's t test.

other tissues, and, indeed, it has been previously shown that this is the case for the kidney (Liu et al., 2018). Overall, the synthesis of NAD^+ from tryptophan is unaltered with age (Figure S2M).

NAD^+ turnover is maintained with age

To investigate the effect of aging on NAD^+ synthesis from circulating NAM, we next infused [2,4,5,6-^{2}H]NAM at a constant rate of 0.2 nmol/g/min (Figure 3A). We reasoned that the lower steady-state NAD^+ concentrations in aged animals could be driven by a decline in the activity of biosynthetic enzymes, an increase in the activity of consuming enzymes, or both. Metabolic flux tends to resist changes in the concentration of a given metabolite, i.e., a fall in NAD^+ concentration favors synthesis (due to a lack of feedback inhibition) and disfavors consumption (due to its lower availability as a substrate) (Brand, 1997). In cultured cells, NAD^+ consumption increases linearly with NAD^+ concentration (Liu et al., 2018). Thus, deficient NAD^+ synthesis should cause decreased NAD^+ turnover (lower concentration and lower consumption), while increased consumer activity should not (lower concentration with equal or faster consumption). Infusion of labeled NAM allows us to distinguish these possibilities.

An advantage of the specific deuterated NAM (M+4) used here is that one of the deuterium atoms is at the redox-active (4-^{2}H) position. This label remains associated with free NAM but is rapidly lost upon incorporation into NAD^+ due to NAD^+/NADH redox cycling. Subsequent cleavage of the labeled NAD^+ releases NAM (M+3). Thus, the appearance of NAM (M+3) in the blood serves as an index of whole-body NAD^+ backbone turnover. Although deuterium labeling can sometimes impact reaction rates (Bush et al., 1973; P, 2011), the chemical position of ^{2}H on these tracers is selected to be far from the reactive atoms involved in NAD^+ synthesis from NAM. Cells co-labeled with [U-^{13}C]NAM and [2,4,5,6-^{2}H]NAM incorporated both tracers into NAD^+ at similar rates, albeit with a slight bias toward the deuterated form (Figure S3A). Based on the positions of the labels, we speculate that this reflects slower incorporation of ^{13}C NAM, rather than a ^{2}H effect, and this is supported by our prior study showing that measurements of [2,4,5,6-^{2}H]NAM incorporation and unlabeled NAD^+ turnover yield the same half-life for NAD^+ (Liu et al., 2018). Nevertheless, we cannot definitively exclude a small kinetic isotope effect. *In vivo*, while the fraction of circulating NAM (M+3) was small and variable at early time points, it was significantly higher in the aged animals by 24 h (Figures 3B, S3B, and S3C), suggesting a net increase in NAD^+ turnover with age, despite the lower NAD^+ concentrations in many tissues.

To determine flux in specific tissues, we next examined the labeling patterns at different times after the start of infusion.

Please cite this article in press as: McReynolds et al., NAD+ flux is maintained in aged mice despite lower tissue concentrations, Cell Systems (2021), https://doi.org/10.1016/j.cels.2021.09.001

CellPress

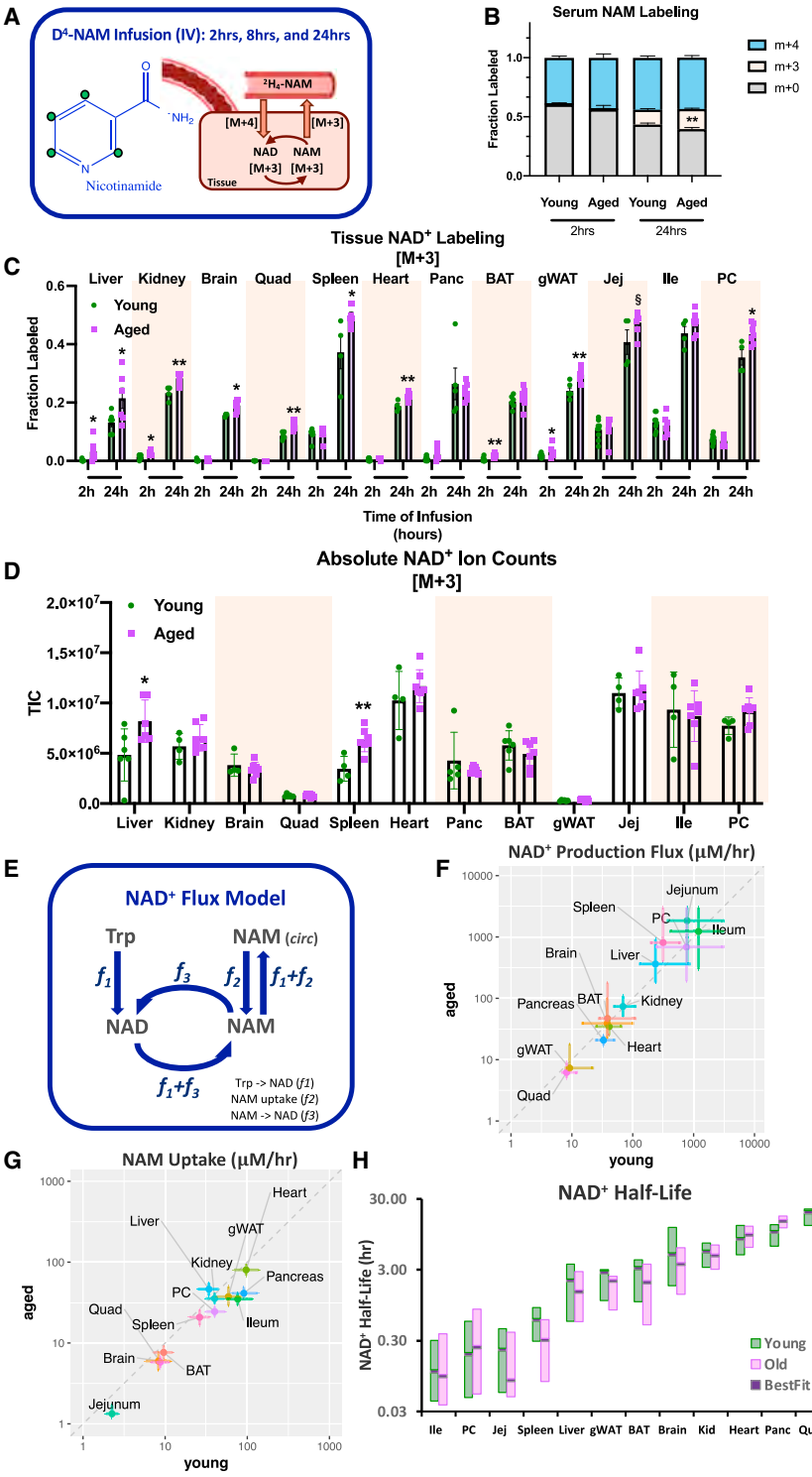

Figure 3. NAD+ turnover is maintained with age

(A) Schematic for experimental design for infusing deuterium-labeled-NAM intravenously in young (3 months) and aged (25 months) C57BL/6 mice.

(B) Fractional labeling of circulating NAM over 2 and 24 h.

(C) Tissue NAD+ labeling over 2 and 24 h.

(D) Absolute ion counts for NAD+ M+3 in young and aged mice after 24 h of labeling.

(E) Schematic illustration of model components for NAD+ flux.

(F) Log-log plot representing NAD+ production fluxes in young and aged tissues.

(G) Log-log plot representing NAM uptake in young and aged mice.

(H) NAD+ labeling half-time across tissues in young and aged mice. Young, n = 6–9; aged, n = 7. For all panels, error bars indicate SEM ***p < 0.001; **p < 0.01; *p < 0.05; §p < 0.1, calculated with Student's t test.

Although M+4 NAM labeling was unaltered, by 24 h, there was an increase in the fractional labeling of recycled NAM (M+3) in the majority of aged tissues (Figures S3D and S3E). Critically, in the majority of the aged tissues, at 24 h, the fractional labeling of NAD+ was also significantly greater in aged mice (Figures 3C and 3D). Similar fractional labeling that increases with aging was also obtained for nicotinamide mononucleotide (NMN) and NADP (Figures S3F and S3G).

To a first approximation, flux is the product of pre-steady-state labeled fraction × pool size. Given the modestly smaller NAD+ pool size in aged tissues (which were preserved after infusion, Figure S3H), our data are consistent with unchanged or slightly increased absolute rates for NAD+ synthesis and breakdown in most tissues (Figures 3C and 3D). To quantitatively model the relationship between fluxes and labeling patterns, we assumed spatial homogeneity and metabolic (but not isotopic) steady-state and considered the key fluxes of tissue NAD+ synthesis from tryptophan (*f*1), tissue NAM uptake from the circulation (*f*2) represents NAM uptake, and tissue NAD+ synthesis from NAM (*f*3) (Figure 3E) (Liu et al., 2018). Tissue NAM production from NAD and excretion to circulation are given by mass balance. For the majority of the young and aged tissues, the model was able to effectively fit the experimentally measured circulating and tissue NAM and NAD+ labeling with respect to time. Total NAD+ turnover flux (sum of f1 + f3) was not significantly different between young and old tissues, with the exception of the pancreas (lower turnover with age) and spleen (higher turnover with age) (Figure 3G; Tables 1 and S1). Thus, NAD+ flux is largely maintained with age despite the lower NAD+ pool sizes in some tissues (Figures 3E and 3F).

A caveat that limits the precision of the modeling is that label incorporation is driven by a combination of NAM uptake and NAD+ flux. When NAD+ flux is fast, relative to NAM uptake, the

Please cite this article in press as: McReynolds et al., NAD+ flux is maintained in aged mice despite lower tissue concentrations, Cell Systems (2021), https://doi.org/10.1016/j.cels.2021.09.001

Table 1. Metabolic flux distributions in young and aged tissues

Tissue	Young (*f1*)	Aged (*f1*)	Young (*f2*)	Aged (*f2*)	Young (*f3*)	Aged (*f3*)
Liver	32.8	34.9*	34.1	46.3*	203.1	327.9*
Kidney	0.7	0.0	40.0	35.5	68.3	73.7
Quad	0.0	0.0*	8.3	6.0*	8.2	6.2*
BAT	0.0	0.0	8.7	5.8*	38.6	46.8
Heart	0.0	0.0	26.3	20.8	40.9	34.6
Spleen	0.4	0.0*	96.8	80.2	315.1	809.8*
Jejunum	0.0	0.0	90.8	41.2*	782.2	1,845.7
Brain	0.0	0.0	9.6	7.7	37.9	39.0
Pancreas	0.0	0.0	58.8	37.4*	33.1	20.8*
gWAT	0.0	0.0	2.3	1.3*	9.2	7.3
Ileum	0.0	0.0	76.4	34.9*	1,203.8	1,232.9
PColon	0.0	0.0	40.1	24.5*	764.1	685.3

Values indicated with an asterisk (*) represent fluxes in the aged mice that significantly improve the fit as compared with assuming no change in the young-mice values. Goodness of fit and significance were evaluated by chi-square test, $\chi^2_{0.05}(df = 3) = 7.8$.

uptake rate (*f2*) becomes the dominant determinant of labeling intensity. Notably, while the NAD+ synthesis flux (f1 + f3) is maintained in most aged tissues, the NAM uptake flux (*f2*) is decreased in many aged tissues (Figure 3G; Table S1). We simulated the labeling patterns of NAD+ and NAM in the aged tissue, assuming that the NAD+ synthesis flux values (f1 + f3) were identical to those of the young animals, and that only the NAM uptake flux (*f2*) changed (Figures S3I and S3J). The simulated labeling data using this method fit the aged tissue labeling patterns as well as when all the three fluxes are allowed to vary, with the exceptions of the spleen and pancreas (Figures S3I and S3J). This suggests that changes in NAM transport may influence NAD+ metabolism in aged tissues. Overall, our data support the maintenance of absolute NAD+ fluxes with age, with tissues that have smaller NAD+ pools sizes turning over those pools modestly faster (Figure 3H).

NAM base exchange is not a major route of label incorporation into NAD+

Several NAD+ consuming enzymes also have the potential to catalyze a base-exchange reaction, whereby free NAM replaces the NAM moiety on NAD+ (Behr et al., 1981; Sauve et al., 1998, 2003). Such reactions have no net consequence to the NAD+ pool within the cell but could result in label transfer, artificially creating the appearance of new NAD+ synthesis, even if it were substantially impaired with age. This mechanism was not a major contributor to NAD+ labeling cultured cells (Liu et al., 2018), since turnover rates calculated based on labeling rates agree with those obtained by inhibiting synthesis. However, base-exchange reactions could still potentially occur *in vivo*.

To test the possibility that the base exchange of the deuterium-labeled NAM with unlabeled NAD+ was confounding our measurements, we performed tracing studies in which young and aged mice were treated with the Nampt inhibitor FK866 prior to infusion (Figures 4A and S4A). Total circulating NAM accumulated in FK866-treated mice, as expected, due to decreased utilization by NAMPT (Figures S4B and S4C). The appearance of M+3 NAM was almost completely abolished in FK866-treated mice, indicating that the majority of NAD+ labeling and subsequent cleavage to make M+3 NAM is a direct result of synthesis by NAMPT, rather than base exchange (Figure 4B). Furthermore, in all tissues, the appearance of labeled NAD+ (M+3) was greatly reduced by FK866, confirming that NAMPT-dependent salvage synthesis, rather than base exchange, accounts for NAD+ labeling from NAM (Figure 4C). As expected, this resulted in significant declines in tissue NAD+ concentrations, with more pronounced effects in tissues with short NAD+ half-lives (Figure 4D). The fractional labeling of NMN, an intermediate in salvage synthesis that would not be labeled by base exchange, was also suppressed (Figures 4E and 4F). Effects of FK866 were consistent across young and aged mice. Thus, our results are not substantially confounded by NAM base exchange and reflect the key *in vivo* NAD+ synthesizing reactions.

Life-long caloric restriction curtails NAD+ turnover

Caloric restriction (CR) can increase lifespan and healthspan (Anderson and Weindruch, 2012; Mattison et al., 2017). Short-term CR treatment increases steady-state NAD+ levels in liver, adipose, and muscle in young rodents (Chen et al., 2008; Song et al., 2014). In muscle, this increase is correlated with upregulation of NAMPT (Song et al., 2014), and key benefits of CR have been attributed to the actions of NAD+-dependent sirtuin enzymes (Chalkiadaki and Guarente, 2012; Chen et al., 2005; Someya et al., 2010), suggesting that CR works in part by driving an increase in NAD+ production and turnover. On the other hand, CR decreases DNA damage and inflammation (Spindler, 2010), which would be expected to decrease NAD+ consumption flux through PARPs and CD38. Thus, in CR, as in aging, NAD+ flux could be predicted to increase or decrease, and the available steady-state measurements are incapable of resolving the question. Therefore, we investigated how NAD+ metabolism was altered in mice subjected to life-long CR.

We infused three groups of animals: young (4 months), aged (24 months), and aged mice subjected to 40% CR from 4 months of age. Similar enrichment of NAM (M+4) was achieved across all three groups (Figure 5A). The appearance of NAM (M+3) in the circulation trended higher with age but was not significantly different between the groups (Figure 5B). In tissues, CR restored NAD+ concentration in the liver and increased it beyond the young level in white adipose tissue (Figure 5C). Newly synthesized M+3 NAD+ appeared slightly more slowly in CR animals, suggesting decreased NAD+ synthesis and turnover (Figure 5D). This was not related to major changes in mRNA expression for PARP1/2 or CD38, indicating changes in posttranscriptional regulation or that other consumers might play a key role (Figures S5G–S5I). NADP+ turnover was also decreased in several tissues in CR animals (Figures 5E and 5F). We further sorted immune cell subsets from the spleen, finding decreased NAD+ levels with aging in B and T cells that were restored by calorie restriction (Figures S5A–S5C). Thus, CR modestly boosts NAD+ levels and curtails NAD+ turnover in multiple aged tissues, suggesting that it suppresses consumer enzyme activity.

Turnover of mitochondrial NAD+

The mitochondrial NAD+ pool is distinct and can sometimes be retained even when nuclear and cytosolic NAD+ are depleted

Please cite this article in press as: McReynolds et al., NAD+ flux is maintained in aged mice despite lower tissue concentrations, Cell Systems (2021), https://doi.org/10.1016/j.cels.2021.09.001

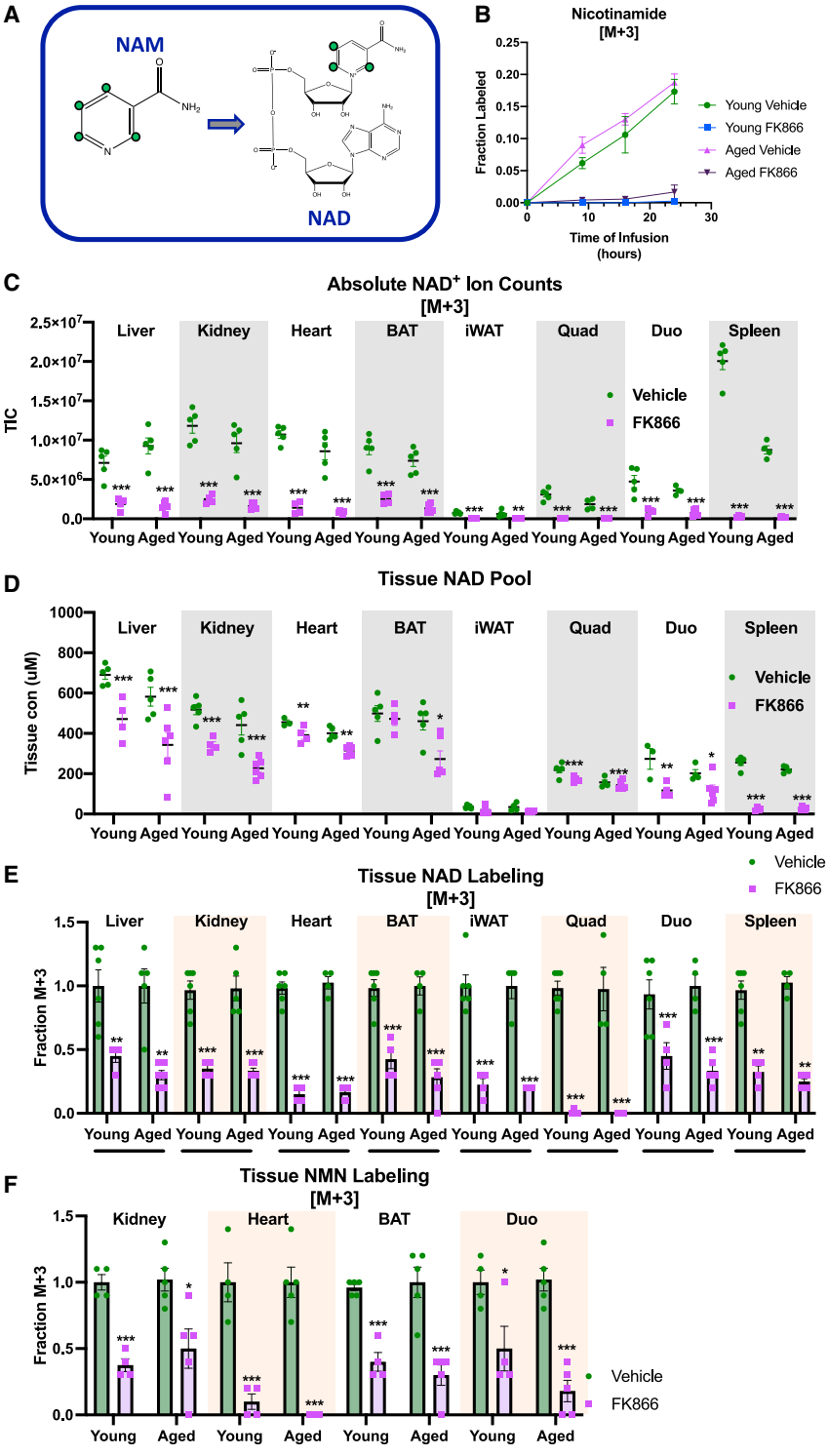

Figure 4. NAM base exchange is not a major route of label incorporation into NAD+

(A) Schematic illustration of the potential of NAD consuming enzymes catalyzing a base-exchange reaction, whereby the free NAM replaces the NAM moiety on NAD+.

(B) Fraction of M+3-labeled NAM in circulation at 9, 16, and 24 h.

(C) Absolute ion counts for NAD+ M+3 in young and aged mice treated with FK866.

(D) Tissue NAD+ pools in young and aged mice after treatment with FK866.

(E) Tissue NAD+ turnover at 24 h of NAM labeling.

(F) Tissue NMN labeling after 24 h of infusing with NAM in young and aged mice treated with FK866. For all panels, error bars indicate SEM ***p < 0.001; **p < 0.01; *p < 0.05; §p < 0.1, calculated with Student's t test.

(Sims et al., 2018; Pittelli et al., 2010; Yang et al., 2007). To determine whether aging and CR have distinct effects on mitochondrial NAD+, we isolated mitochondria from the liver, kidney, and quadriceps muscles. NAD+ levels in the mitochondria were not significantly decreased with age but trended lower in the skeletal muscle and kidney (Figures S5D–S5F). Total mitochondrial NAD+ content was significantly increased by CR only in the liver. Labeling patterns for mitochondrial NAD+ almost perfectly mirrored those in bulk tissues, except that the fractional labeling was 10%–20% lower in each case (Figure 5H). This is consistent with NAD+ being made in the cytosol and imported in mitochondria, with substantial but incomplete equilibration between the two compartments (Davila et al., 2018; Girardi et al., 2020; Kory et al., 2020; Luongo et al., 2020).

NAD+ pool resiliency with age

Under basal conditions, NAD+ flux is maintained in aged mice. But what happens under conditions of stress? Lipopolysaccharide (LPS) elicits a systemic inflammatory response and depletes NAD+ in immune cells and tissues (Figures 6A, 6B, and S6A–S6E) (Chini et al., 2020; Covarrubias et al., 2020; Moreno-Vinasco et al., 2014). This was associated with increases in circulating NAM and its catabolites after LPS treatment (Figure 6C and S6F–S6J; Table 2) (Hayat et al., 2021), and we noted increased mRNA expression of CD38 in the kidney and a trending increase in the liver (Figures S6K and S6L). NAM accumulation can reflect either increased NAD+ breakdown or slower NAD+ synthesis. The use of tracers allows us to make the distinction since the faster breakdown of NAD+ should dilute the labeling of the infused NAM M+4 pool by releasing more unlabeled NAM or NAM M+3. Instead, upon LPS treatment, we observed that the fraction of NAM+4 was maintained or even slightly increased as total NAM rose (Figure 6D). Consistent with the accumulation of NAM reflecting impaired consumption for NAD synthesis, both the total abundance and the M+4 fractional labeling of NAM increased substantially in the tissues of

Please cite this article in press as: McReynolds et al., NAD+ flux is maintained in aged mice despite lower tissue concentrations, Cell Systems (2021), https://doi.org/10.1016/j.cels.2021.09.001

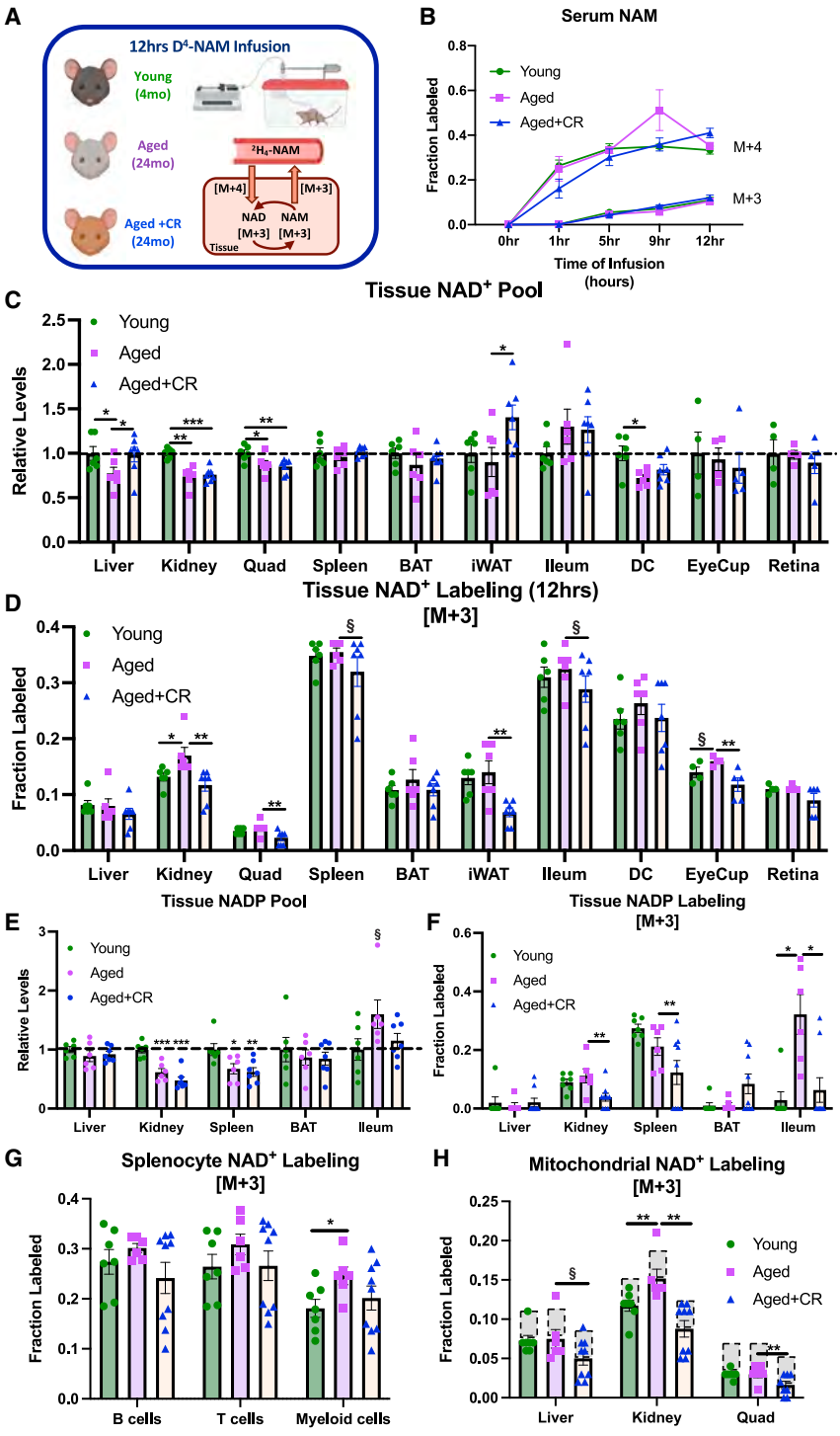

Figure 5. Calorie restriction moderately increases NAD+ pools and decreases turnover in subsets of tissues

(A) Schematic for experimental design.
(B) Fraction of circulating NAM labeled over 12 h in young, aged, and aged +CR mice.
(C) Tissue NAD+ pools in young, aged, and aged +CR mice.
(D) Tissue NAD+ turnover at 12 h of NAM labeling.
(E) Tissue NADP pools in young, aged, and aged +CR mice.
(F) Tissue NADP labeling after 12 h in young, aged, and aged +CR mice.
(G) Splenocyte NAD+ turnover from circulating NAM.
(H) Mitochondria NAD+ turnover from circulating NAM—gray bars represent bulk tissue labeling. Young, n = 6; aged, n = 6; aged+CR, n = 7. For all panels, error bars indicate SEM ***p < 0.001; **p < 0.01; *p < 0.05; §p < 0.1, calculated with Student's t test.

LPS-treated mice, regardless of age (Figure 6E). Despite the higher fractional labeling of NAM in tissues, labeling of NAD+ was similar or decreased after LPS treatment, further supporting slower NAD+ synthesis from NAM (Figures 6F–6H). These effects were also consistent between young and old animals, which overall showed similar resiliency of their total tissue NAD+ pools and labeling in response to the LPS stress. Thus, in contrast to aging, which modestly depletes NAD+, likely via a chronic subtle increase in consumer activity, LPS triggers NAD+ depletion by acutely impairing synthesis.

DISCUSSION

NAD+ is crucial to the maintenance of cellular homeostasis, with roles in energy balance, stress responses, epigenetics, DNA repair, immune responses, and a host of metabolic reactions. Hence, perturbations to the NAD+ pool have the potential to trigger accelerated metabolic decline and may contribute to age-associated aliments (Mills et al., 2016; Zhang et al., 2016). Although age-related NAD+ decline has been documented in numerous studies, there is no clear consensus as to the underlying causes, or even whether the primary driver is increased consumption or impaired synthesis. Here, we analyze the impact of age on NAD+ metabolic fluxes in mice, finding evidence for the decline in NAD+ pool size with age being the result of chronic and subtle increases in consumer activity, with maintained production fluxes. We note that while some prior studies have reported more dramatic NAD+ loss with age, others are in line with our estimates (Yoshino et al., 2018) and that there may be some publication bias toward positive results in addition to differences due to the diets, species, and strains being studied.

Which consumers are driving the NAD+ decline with aging? Two leading candidates from the literature are CD38 (more active due to inflammatory changes) and PARP1 (activated by DNA damage). But many NAD+ consuming enzymes remain poorly characterized *in vivo*. For example, the activities of most mono-ADP-ribosyltransferases have been difficult to study until

Please cite this article in press as: McReynolds et al., NAD+ flux is maintained in aged mice despite lower tissue concentrations, Cell Systems (2021), https://doi.org/10.1016/j.cels.2021.09.001

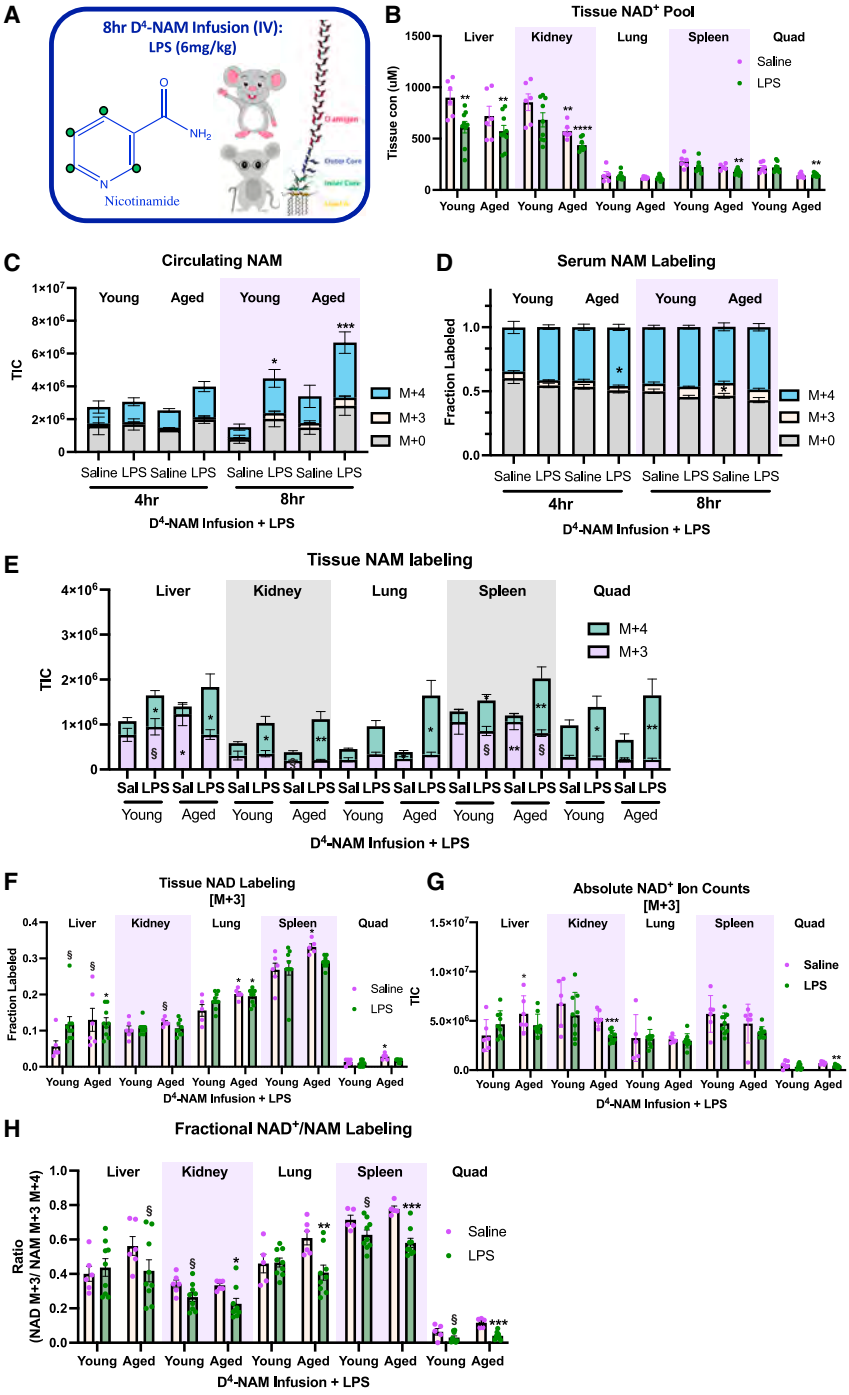

Figure 6. Acute inflammatory stress decreases NAD+ synthesis

(A) Schematic for experimental design for infusing deuterium-labeled-NAM intravenously in young (3 months) and aged (25 months) C57BL/6 mice treated with LPS (6 mg/kg) exposure.

(B) Tissue NAD+ pools in young and aged mice treated with LPS.

(C) Circulating NAM levels at 4 and 8 h after infusion.

(D) Fraction circulating NAM over the 8 h infusion.

(E) Tissue NAM labeling after 8 h deuterium NAM infusion.

(F) Tissue NAD+ labeling over 8 h in young and aged mice treated with LPS.

(G) Absolute ion counts for NAD+ M+3 in young and aged mice treated with LPS.

(H) Ratio of tissue NAD M+3 and the sum of NAM M+3 and M+4. Young saline, n = 6; young LPS, n = 9; aged saline, n = 6; aged LPS, n = 9. For all panels, error bars indicate SEM ****p < 0.0005; ***p < 0.001; **p < 0.01; *p < 0.05; §p < 0.1, calculated with Student's t test.

recently due to the lack of reagents that could detect the mono-ADP-ribosyl modification on proteins, and SARM1 has been the subject of intense scrutiny within axons but its roles in other tissues remain underexplored. Notably, increased activity of any one NAD+ consumer is expected to correspondingly decrease flux through other consumers by limiting the steady-state NAD+ concentration. Such competition has previously been described for CD38 (Aksoy et al., 2006) and PARP (Bai et al., 2011), each of which can limit the activity of sirtuins. A high priority moving forward is to understand in more detail how the activities of individual NAD+ consuming enzymes change across the lifespan.

Another important consideration for future study is the potential for heterogeneity at the cellular or even subcellular level. While our data suggest increased consumer activity as the general paradigm driving the age-related decline in NAD+ in most tissues, impaired synthesis has been implicated in the aging of specific cell types, including loss of tryptophan-dependent synthesis in macrophages (Minhas et al., 2019), loss of NMNAT-2 dependent synthesis in aged oocytes (Wu et al., 2019), and diminished delivery of circulating NAMPT to the aging hypothalamus where it can influence tissue NAD+ levels (Yoshida et al., 2019). Our methodology does not resolve such effects. Moreover, NAD+ is compartmentalized into multiple subcellular pools (Dölle et al., 2010) that have not been investigated in aging. Here we provide, to our knowledge, the first data on stable isotope tracing of NAM into mitochondrial NAD+ pools *in vivo*. In the tissues and conditions studied, mitochondrial NAD+ labeling patterns tended to closely follow those of bulk tissue, albeit with 10%–20% less total labeling as compared with the parent tissue under any given condition. This is consistent with our previous observation that intact cytosolic NAD+ can enter the mitochondria (Davila et al., 2018). However, the mitochondrial pool can behave in a distinct manner under conditions of NAD+ depletion or stress (Pittelli et al., 2010; Sims et al., 2018; Yang et al., 2007), and numerous other subcellular compartments remain uninvestigated. Therefore, our data provide a framework for studying systemic changes in NAD+ metabolism with age, but many details

Please cite this article in press as: McReynolds et al., NAD+ flux is maintained in aged mice despite lower tissue concentrations, Cell Systems (2021), https://doi.org/10.1016/j.cels.2021.09.001

Table 2. NAM catabolites are induced in LPS-treated mice

mNAM: tissue	Young LPS/ young saline	Aged saline/ young saline	Aged LPS/ aged saline
Liver	1.67 ± 1.34	0.74 ± 0.18	1.15 ± 0.29
Kidney	3.01± 1.56	1.84 ± 0.88	9.77 ± 6.99
Lung	1.34 ± 0.79	0.63 ± 0.10*	0.89 ± 0.21*
Spleen	1.09 ± 0.72	0.60 ± 0.09	0.75 ± 0.18
Quad	1.06 ± 0.68	0.36 ± 0.06*	0.55 ± 0.11*
N-Me-4PY: tissue			
Liver	1.86 ± 1.09	0.48 ± 0.31*	1.55 ± 0.94*
Kidney	3.02 ± 1.23*	1.23 ± 0.71	3.57 ± 2.10*
Lung	3.44 ± 1.74*	0.63 ± 0.20	3.94 ± 1.99*
Spleen	3.86 ± 2.07	0.80 ± 0.14	3.84 ± 1.67*
Quad	1.69 ± 0.97	0.39 ± 0.15	1.65 ± 0.92*
N-Me-6PY: tissue			
Liver	2.85 ± 2.73	1.01 ± 0.98	2.99 ± 3.22
Kidney	2.77 ± 1.37*	1.25 ± 1.07	3.10 ± 1.76*
Lung	3.38 ± 2.03*	0.52 ± 0.41	2.62 ± 1.77*
Spleen	3.21 ± 2.10*	0.62 ± 0.66	2.61 ± 2.61
Quad	1.34 ± 0.74	0.25 ± 0.11	2.10 ± 1.25*
4PY: tissue			
Liver	3.42 ± 1.77*	0.66 ± 0.20	3.51 ± 2.12*
Kidney	3.16 ± 1.87*	1.25 ± 0.92	3.73 ± 2.33*
Lung	3.54 ± 2.11*	0.62 ± 0.23	4.01 ± 2.47*
Spleen	3.30 ± 1.74*	0.85 ± 0.28	3.69 ± 2.33*
Quad	1.13 ± 0.58	0.42 ± 0.16	1.52 ± 0.88*
6PY: tissue			
Liver	2.07 ± 2.07	0.44 ± 0.13	1.97 ± 1.53*
Kidney	2.17 ± 1.09*	0.91 ± 0.56	2.12 ± 1.48
Lung	2.63 ± 1.55*	0.53 ± 0.18	3.14 ± 2.09*
Spleen	2.36 ± 1.42*	0.61 ± 0.26*	2.15 ± 1.51*
Quad	1.09 ± 0.50	0.39 ± 0.18	1.00 ± 0.58

Values indicated with an asterisk (*) represent the ratios that are significantly altered in LPS-treated or aged mice (fold-change ± SD).

remain to be elucidated with respect to the dynamics of NAD+ at the level of individual cells and organelles.

While we find that the average basal rates of NAD+ synthesis do not change appreciably with age in most tissues, we do not exclude the possibility that the *capacity* for NAD+ biosynthesis is diminished. This could become an important limitation under conditions of stress, such as DNA damage, that drives acute consumption of NAD+. Moreover, it may be the case that even the basal activity of some NAD+ biosynthetic enzymes decreases slightly with age, but that the decrease in steady-state NAD+ concentration relieves feedback inhibition to restore normal flux. Indeed, NAMPT is subject to feedback inhibition by NAD+ (Dietrich et al., 1968), and the mild phenotypes of heterozygous animals (Revollo et al., 2007) suggest that its capacity is in excess of what is used under basal conditions. However, our efforts to induce NAD+ limitation stress with LPS did not augment differences between young and aged animals and instead revealed that LPS decreases NAD+ synthesis similarly across the lifespan.

An alternative form of stress is calorie restriction. Consistent with calorie restriction being anti-aging, it restored NAD+ concentration in aged liver and adipose. Contrary to the view that calorie restriction boosts NAD+ levels via increasing synthesis (Song et al., 2014; Fulco et al., 2008; Wei et al., 2020), we observed relatively strong decreases in NAD+ turnover. This may reflect broader alterations of metabolism, for example, limited production of phosphoribosylpyrophosphate, a product of the pentose phosphate pathway that is required for nucleotide synthesis (Lane and Fan, 2015). During LPS treatment, NAD+ production may be limited for similar reasons since glucose concentrations fall, which likely reduces flux into the pentose phosphate pathway (Irahara et al., 2018; Vogel et al., 1991). But ultimately the outcomes are different, as calorie restriction (but not LPS) offsets any decrease in NAD+ production by suppressing consumption.

Our findings have implications for NAD+ supplementation. If synthesis rates were impaired with age, then restoring NAD+ production with supplements, such as nicotinamide riboside or mononucleotide, or pharmacological strategies, such as NAMPT activation (Gardell et al., 2019), would simply be restoring normal "youthful" physiology. However, our data suggest that such strategies would act by boosting synthesis rates beyond normal in the face of increased consumption. This may alleviate the NAD+ shortage for redox reactions and enzymes such as sirtuins. However, it also increases NAD+ availability to any enzymes that might be hyperactivated with age. The consequences of chronically driving more activation of PARPs or CD38 are not entirely clear but should be considered. On an optimistic note, the worst consequence of PARP1 hyperactivation may well be NAD+ depletion (Scheibye-Knudsen et al., 2014), which is not an issue if the excess activity is driven by NAD+ oversupply. Determining NAD+ turnover rates and flux through specific consumer pathways in animals with artificially elevated tissue NAD+ concentrations is an important future direction.

In summary, we provide the first direct measurements of age-related changes in NAD+ turnover, finding that production is not impaired by aging. Instead, our data suggest that, with age, increased consumption drives modest declines in NAD+ concentrations. The findings are particularly germane given the possibility of targeting NAD+ metabolism to ameliorate age-related diseases.

STAR★METHODS

Detailed methods are provided in the online version of this paper and include the following:

- KEY RESOURCES TABLE
- RESOURCE AVAILABILITY
  - Lead contact
  - Materials availability
  - Data and code availability
- EXPERIMENTAL MODEL AND SUBJECT DETAILS
  - Animal use and care
- METHOD DETAILS
  - Intravenous infusion of mice
  - Metabolite extraction from serum and tissues
  - NAD measurement by enzymatic cycling assay

- Immune cell sorting and metabolite extraction
- Extraction of Mitochondrial Metabolites
- Metabolite measurement

- QUANTIFICATION AND STATISTICAL ANALYSIS
  - Quantification of NAD+ Fluxes *In Vivo*
  - Statistical analysis

SUPPLEMENTAL INFORMATION

Supplemental information can be found online at https://doi.org/10.1016/j.cels.2021.09.001.

ACKNOWLEDGMENTS

This work was funded and supported by both the Howard Hughes Medical Institute and Burroughs Wellcome Fund via the PDEP and Hanna H. Gray Fellow Programs awarded to M.R.M.; Crohn's and Colitis Career Development Award to K.C.; and NIH grants CA211437 to W.L., DP1DK113643 to J.D.R., and R01DK098656 and R01AG043483 to J.A.B. We thank Ophir Shalem (CHOP) for support with cell sorting. Furthermore, we acknowledge support from the Regional Metabolomics and Fluxomics Core and the Rodent Metabolic Phenotyping Core of the Penn Diabetes Research Center P30-DK19525, the CINJ Cancer Center Support Grant, and the Rutgers Cancer Institute of New Jersey Metabolomics Shared Resource, supported, in part, with funding from NCI-CCSG P30CA072720-5923.

AUTHOR CONTRIBUTIONS

M.R.M., K.C., J.D.R., and J.A.B. conceived the project. M.R.M. and K.C. conceived all experiments. M.R.M. and K.C. performed and analyzed most experiments. M.R.M. and X.S. conducted the flux analysis. M.R.M., K.C., W.L., E.C., C.J., Y.S., L.C., H.C.D., S.M., Y.R.B., Q.C., X.J., F.S., and P.B. performed specific *in vivo* experiments and analyses. M.R.M. and J.A.B. wrote the manuscript with input from all authors.

DECLARATION OF INTERESTS

J.D.R. and J.A.B. are consultants to Pfizer. J.D.R. is an advisor and stock owner in Colorado Research Partners, L.E.A.F. Pharmaceuticals, Rafael Pharmaceuticals, Raze Therapeutics, Kadmon Pharmaceuticals, and Agios pharmaceuticals. J.D.R. is a co-inventor of SHIN2 and related SHMT inhibitors, which have been patented by Princeton University, and is a co-founder of Toran Therapeutics. G.X., M.F.C., and G.J.T. are current or former employees of Pfizer who may hold Pfizer stock and/or stock options. J.A.B. and S.M. are inventors on a patent for using NAD+ precursors in liver injury and have received research funding and materials from Elysium Health and Metro International Biotech, both of which have an interest in NAD+ precursors. The remaining authors have nothing to declare.

INCLUSION AND DIVERSITY

One or more of the authors of this paper self-identifies as an underrepresented ethnic minority in science. One or more of the authors of this paper received support from a program designed to increase minority representation in science. While citing references scientifically relevant for this work, we also actively worked to promote gender balance in our reference list.

Received: July 28, 2020
Revised: June 8, 2021
Accepted: August 31, 2021
Published: September 23, 2021

REFERENCES

Adusumilli, R., and Mallick, P. (2017). Data conversion with ProteoWizard msConvert. Methods Mol. Biol. *1550*, 339–368.

Aksoy, P., Escande, C., White, T.A., Thompson, M., Soares, S., Benech, J.C., and Chini, E.N. (2006). Regulation of SIRT 1 mediated NAD dependent deacetylation: a novel role for the multifunctional enzyme CD38. Biochem. Biophys. Res. Commun. *349*, 353–359.

Amici, S.A., Young, N.A., Narvaez-Miranda, J., Jablonski, K.A., Arcos, J., Rosas, L., Papenfuss, T.L., Torrelles, J.B., Jarjour, W.N., and Guerau-de-Arellano, M. (2018). CD38 is robustly induced in human macrophages and monocytes in inflammatory conditions. Front. Immunol. *9*, 1593.

Anderson, R.M., and Weindruch, R. (2012). The caloric restriction paradigm: implications for healthy human aging. Am. J. Hum. Biol. *24*, 101–106.

Antoniewicz, M.R., Kelleher, J.K., and Stephanopoulos, G. (2006). Determination of confidence intervals of metabolic fluxes estimated from stable isotope measurements. Metab. Eng. *4*, 324–337.

Bai, P., Cantó, C., Oudart, H., Brunyánszki, A., Cen, Y., Thomas, C., Yamamoto, H., Huber, A., Kiss, B., Houtkooper, R.H., et al. (2011). PARP-1 inhibition increases mitochondrial metabolism through SIRT1 activation. Cell Metab. *13*, 461–468.

Behr, A., Taguchi, H., and Gholson, R.K. (1981). Apparent pyridine nucleotide synthesis in mitochondria: an artifact of NMN and NAD glycohydrolase activity? Biochem. Biophys. Res. Commun. *101*, 767–774.

Braidy, N., Guillemin, G.J., Mansour, H., Chan-Ling, T., Poljak, A., and Grant, R. (2011). Age related changes in NAD+ metabolism oxidative stress and Sirt1 activity in Wistar rats. PLoS One *6*, e19194.

Brand, M.D. (1997). Regulation analysis of energy metabolism. J. Exp. Biol. *200*, 193–202.

Bush, K., Shiner, V.J., and Mahler, H.R. (1973). Deuterium isotope effects on initial rates of the liver alcohol dehydrogenase reaction. Biochemistry *6*, 4802–4805.

Camacho-Pereira, J., Tarragó, M.G., Chini, C.C.S., Nin, V., Escande, C., Warner, G.M., Puranik, A.S., Schoon, R.A., Reid, J.M., Galina, A., and Chini, E.N. (2016). CD38 dictates age-related NAD decline and mitochondrial dysfunction through an SIRT3-dependent mechanism. Cell Metab. *23*, 1127–1139.

Chalkiadaki, A., and Guarente, L. (2012). Sirtuins mediate mammalian metabolic responses to nutrient availability. Nat. Rev. Endocrinol. *8*, 287–296.

Chen, D., Bruno, J., Easlon, E., Lin, S.J., Cheng, H.L., Alt, F.W., and Guarente, L. (2008). Tissue-specific regulation of SIRT1 by calorie restriction. Genes Dev. *22*, 1753–1757.

Chen, D., Steele, A.D., Lindquist, S., and Guarente, L. (2005). Increase in activity during calorie restriction requires Sirt1. Science *310*, 1641.

Chini, C., Hogan, K.A., Warner, G.M., Tarragó, M.G., Peclat, T.R., Tchkonia, T., Kirkland, J.L., and Chini, E. (2019). The NADase CD38 is induced by factors secreted from senescent cells providing a potential link between senescence and age-related cellular NAD+ decline. Biochem. Biophys. Res. Commun. *513*, 486–493.

Chini, C.C.S., Peclat, T.R., Warner, G.M., Kashyap, S., Espindola-Netto, J.M., de Oliveira, G.C., Gomez, L.S., Hogan, K.A., Tarragó, M.G., Puranik, A.S., et al. (2020). CD38 ecto-enzyme in immune cells is induced during aging and regulates NAD+ and NMN levels. Nat. Metab. *2*, 1284–1304.

Chini, C.C.S., Tarragó, M.G., and Chini, E.N. (2017). NAD and the aging process: role in life, death and everything in between. Mol. Cell. Endocrinol. *455*, 62–74.

Clement, J., Wong, M., Poljak, A., Sachdev, P., and Braidy, N. (2019). The plasma NAD+ metabolome is dysregulated in "normal" aging. Rejuvenation Res. *22*, 121–130.

Covarrubias, A.J., Kale, A., Perrone, R., Lopez-Dominguez, J.A., Pisco, A.O., Kasler, H.G., Schmidt, M.S., Heckenbach, I., Kwok, R., Wiley, C.D., et al. (2020). Senescent cells promote tissue NAD+ decline during ageing via the activation of CD38+ macrophages. Nat. Metab. *2*, 1265–1283.

Davila, A., Liu, L., Chellappa, K., Redpath, P., Nakamaru-Ogiso, E., Paolella, L.M., Zhang, Z., Migaud, M.E., Rabinowitz, J.D., and Baur, J.A. (2018). Nicotinamide adenine dinucleotide is transported into mammalian mitochondria. eLife *7*, e33246.

Dietrich, L.S., M.O., and Powanda, M. (1968). NAD synthesis in animal tissues. J. Vitaminol. (Kyoto) *14*, 123–129.

Dölle, C., Niere, M., Lohndal, E., and Ziegler, M. (2010). Visualization of subcellular NAD pools and intra-organellar protein localization by poly-ADP-ribose formation. Cell. Mol. Life Sci. *67*, 433–443.

Fang, E.F., Scheibye-Knudsen, M., Brace, L.E., Kassahun, H., SenGupta, T., Nilsen, H., Mitchell, J.R., Croteau, D.L., and Bohr, V.A. (2014). Defective mitophagy in XPA via PARP-1 hyperactivation and NAD+/SIRT1 reduction. Cell *157*, 882–896.

Frederick, D.W., Davis, J.G., Dávila, A.J., Agarwal, B., Michan, S., Puchowicz, M.A., Nakamaru-Ogiso, E., and Baur, J.A. (2015). Increasing NAD synthesis in muscle via nicotinamide phosphoribosyltransferase is not sufficient to promote oxidative Metabolism. J. Biol. Chem. *290*, 1546–1558.

Fulco, M., Cen, Y., Zhao, P., Hoffman, E.P., McBurney, M.W., Sauve, A.A., and Sartorelli, V. (2008). Glucose restriction inhibits skeletal myoblast differentiation by activating SIRT1 through AMPK-mediated regulation of Nampt. Dev. Cell *14*, 661–673.

Gardell, S.J., Hopf, M., Khan, A., Dispagna, M., Sessions, H.E., Falter, R., Kapoor, N., Brooks, J., Culver, J., Petucci, C., et al. (2019). Boosting NAD+ with a small molecule that activates NAMPT. Nat. Commun. *10*, 3241.

Girardi, E., Agrimi, G., Goldmann, U., Fiume, G., Lindinger, S., Sedlyarov, V., Srndic, I., Gürtl, B., Agerer, B., Kartnig, F., et al. (2020). Epistasis-driven identification of SLC25A51 as a regulator of human mitochondrial NAD import. Nat. Commun. *11*, 6145.

Gomes, A.P., Price, N.L., Ling, A.J.Y., Moslehi, J.J., Montgomery, M.K., Rajman, L., White, J.P., Teodoro, J.S., Wrann, C.D., Hubbard, B.P., et al. (2013). Declining NAD+ induces a pseudohypoxic state disrupting nuclear103 mitochondrial communication during aging. Cell *155*, 1624–1638.

Guan, Y., Wang, S.R., Huang, X.Z., Xie, Q.H., Xu, Y.Y., Shang, D., and Hao, C.M. (2017). Nicotinamide mononucleotide, an NAD+ precursor, rescues age-associated susceptibility to AKI in a sirtuin 1-dependent manner. J. Am. Soc. Nephrol. *28*, 2337–2352.

Hayat, F., Sonavane, M., Makarov, M.V., Trammell, S.A.J., McPherson, P., Gassman, N.R., and Migaud, M.E. (2021). The biochemical pathways of nicotinamide-derived pyridones. Int. J. Mol. Sci. *22*, 1145.

Irahara, T., Sato, N., Otake, K., Matsumura, S., Inoue, K., Ishihara, K., Fushiki, T., and Yokota, H. (2018). Alterations in energy substrate metabolism in mice with different degrees of sepsis. J. Surg. Res. *227*, 44–51.

Kang, B.N., Tirumurugaan, K.G., Deshpande, D.A., Amrani, Y., Panettieri, R.A., Walseth, T.F., and Kannan, M.S. (2006). Transcriptional regulation of CD38 expression by tumor necrosis factor-alpha in human airway smooth muscle cells: role of NF-kappaB and sensitivity to glucocorticoids. FASEB J. *20*, 1000–1002.

Kory, N., Uit de Bos, J.U., van der Rijt, S., Jankovic, N., Güra, M., Arp, N., Pena, I.A., Prakash, G., Chan, S.H., Kunchok, T., et al. (2020). MCART1/SLC25A51 is required for mitochondrial NAD transport. Sci. Adv. *6*, eabe5310.

Lane, A.N., and Fan, T.W. (2015). Regulation of mammalian nucleotide metabolism and biosynthesis. Nucleic Acids Res. *43*, 2466–2485.

Liu, L.,S.X., Quinn, W.J., Hui, S., Krukenberg, K., Frederick, D.W., Redpath, P., Zhan, L., Chellappa, K., White, E., et al. (2018). Quantitative analysis of NAD synthesis-breakdown fluxes. Cell Metab. *27*, 1067–1080.e5.

Lu, W., Wang, L., Chen, L., Hui, S., and Rabinowitz, J.D. (2018). Extraction and quantitation of nicotinamide adenine dinucleotide redox cofactors. Antioxid. Redox Signal. *28*, 167–179.

Luongo, T.S., Eller, J.M., Lu, M.J., Niere, M., Raith, F., Perry, C., Bornstein, M.R., Oliphint, P., Wang, L., McReynolds, M.R., et al. (2020). SLC25A51 is a mammalian mitochondrial NAD+ transporter. Nature *588*, 174–179.

Massudi, H., Grant, R., Braidy, N., Guest, J., Farnsworth, B., and Guillemin, G.J. (2012). Age-associated changes in oxidative stress and NAD+ metabolism in human tissue. PLoS One *7*, e42357.

Matalonga, J., Glaria, E., Bresque, M., Escande, C., Carbó, J.M., Kiefer, K., Vicente, R., León, T.E., Beceiro, S., Pascual-García, M., et al. (2017). The nuclear receptor LXR limits bacterial infection of host macrophages through a mechanism that impacts cellular NAD metabolism. Cell Rep. *18*, 1241–1255.

Mattison, J.A., Colman, R.J., Beasley, T.M., Allison, D.B., Kemnitz, J.W., Roth, G.S., Ingram, D.K., Weindruch, R., de Cabo, R., and Anderson, R.M. (2017). Caloric restriction improves health and survival of rhesus monkeys. Nat. Commun. *8*, 14063.

McReynolds, M.R., Chellappa, K., and Baur, J.A. (2020). Age-related NAD+ decline. Exp. Gerontol. *134*, 110888.

Mills, K.F., Yoshida, S., Stein, L.R., Grozio, A., Kubota, S., Sasaki, Y., Redpath, P., Migaud, M.E., Apte, R.S., Uchida, K., et al. (2016). Long-term administration of nicotinamide mononucleotide mitigates age-associated physiological decline in mice. Cell Metab. *24*, 795–806.

Minhas, P.S., Liu, L., Moon, P.K., Joshi, A.U., Dove, C., Mhatre, S., Contrepois, K., Wang, Q., Lee, B.A., Coronado, M., et al. (2019). Macrophage de novo NAD+ synthesis specifies immune function in aging and inflammation. Nat. Immunol. *20*, 50–63.

Mitchell, S.J., Bernier, M., Aon, M.A., Cortassa, S., Kim, E.Y., Fang, E.F., Palacios, H.H., Ali, A., Navas-Enamorado, I., Di Francesco, A., Kaiser, T.A., et al. (2018). Nicotinamide improves aspects of healthspan, but not lifespan, in mice. Cell Metab. *6*, 667–676.e4.

Moreno-Vinasco, L., Quijada, H., Sammani, S., Siegler, J., Letsiou, E., Deaton, R., Saadat, L., Zaidi, R.S., Messana, J., Gann, P.H., et al. (2014). Nicotinamide phosphoribosyltransferase inhibitor is a novel therapeutic candidate in murine models of inflammatory lung injury. Am. J. Respir. Cell Mol. Biol. *51*, 223–228.

Mouchiroud, L., Houtkooper, R.H., and Auwerx, J. (2013). NAD+ metabolism: a therapeutic target for age-related metabolic disease. Crit. Rev. Biochem. Mol. Biol. *48*, 397–408.

Musso, T., Deaglio, S., Franco, L., Calosso, L., Badolato, R., Garbarino, G., Dianzani, U., and Malavasi, F. (2001). CD38 expression and functional activities are up-regulated by IFN-gamma on human monocytes and monocytic cell lines. J. Leukoc. Biol. *69*, 605–612.

Pittelli, M., Formentini, L., Faraco, G., Lapucci, A., Rapizzi, E., Cialdai, F., Romano, G., Moneti, G., Moroni, F., and Chiarugi, A. (2010). Inhibition of nicotinamide phosphoribosyltransferase: cellular bioenergetics reveals a mitochondrial insensitive NAD pool. J. Biol. Chem. *285*, 34106–34114.

Pollak, N., Dölle, C., and Ziegler, M. (2007). The power to reduce: pyridine nucleotides – small molecules with a multitude of functions. Biochem. J. *402*, 205–218.

Revollo, J.R., Körner, A., Mills, K.F., Satoh, A., Wang, T., Garten, A., Dasgupta, B., Sasaki, Y., Wolberger, C., Townsend, R.R., et al. (2007). Nampt/PBEF/Visfatin regulates insulin secretion in beta cells as a systemic NAD biosynthetic enzyme. Cell Metab. *6*, 363–375.

Salvatori, I., Valle, C., Ferri, A., and Carrì, M.T. (2017). SIRT3 and mitochondrial metabolism in neurodegenerative diseases. Neurochem. Int. *109*, 184–192.

Sauve, A.A., Munshi, C., Lee, H.C., and Schramm, V.L. (1998). The reaction mechanism for CD38. A single intermediate is responsible for cyclization, hydrolysis, and base-exchange chemistries. Biochemistry *37*, 13239–13249.

Sauve, A.A., and Schramm, V.L. (2003). Sir2 regulation by nicotinamide results from switching between base exchange and deacetylation chemistry. Biochemistry *42*, 9249–9256.

Scheibye-Knudsen, M., Mitchell, S.J., Fang, E.F., Iyama, T., Ward, T., Wang, J., Dunn, C.A., Singh, N., Veith, S., Hasan-Olive, M.M., et al. (2014). A high-fat diet and NAD(+) activate Sirt1 to rescue premature aging in Cockayne syndrome. Cell Metab *20*, 840–855.

Shibata, K. (2018). Organ co-relationship in tryptophan metabolism and factors that govern the biosynthesis of nicotinamide from tryptophan. J. Nutr. Sci. Vitaminol. (Tokyo) *64*, 90–98.

Sims, C.A., Guan, Y., Mukherjee, S., Singh, K., Botolin, P., Davila, A., Jr., and Baur, J.A. (2018). Nicotinamide mononucleotide preserves mitochondrial function and increases survival in hemorrhagic shock. JCI Insight *3*, e120182.

Someya, S., Yu, W., Hallows, W.C., Xu, J., Vann, J.M., Leeuwenburgh, C., Tanokura, M., Denu, J.M., and Prolla, T.A. (2010). Sirt3 mediates reduction of oxidative damage and prevention of age-related hearing loss under caloric restriction. Cell *143*, 802–812.

Song, J., Ke, S.F., Zhou, C.C., Zhang, S.L., Guan, Y.F., Xu, T.Y., Sheng, C.Q., Wang, P., and Miao, C.Y. (2014). Nicotinamide phosphoribosyltransferase is required for the calorie restriction-mediated improvements in oxidative stress,

mitochondrial biogenesis, and metabolic adaptation. J. Gerontol. A Biol. Sci. Med. Sci. *69*, 44–57.

Spindler, S.R. (2010). Caloric restriction: from soup to nuts. Ageing Res. Rev. *9*, 324–353.

Srivastava, S. (2016). Emerging therapeutic roles for NAD+ metabolism in mitochondrial and age-related disorders. Clin. Transl. Med. *5*, 25.

Stein, L.R., and Imai, S. (2014). Specific ablation of Nampt in adult neural stem cells recapitulates their functional defects during aging. EMBO J. *33*, 1321–1340.

Su, X., Lu, W., and Rabinowitz, J.D. (2017). Metabolite spectral accuracy on orbitraps. Anal. Chem. *89*, 5940–5948.

Tarragó, M.G., Chini, C.C.S., Kanamori, K.S., Warner, G.M., Caride, A., de Oliveira, G.C., Rud, M., Samani, A., Hein, K.Z., Huang, R., et al. (2018). A potent and specific CD38 inhibitor ameliorates age-related metabolic dysfunction by reversing tissue NAD+ decline. Cell Metab. *27*, 1081–1095.e10.

Ubaida-Mohien, C., Lyashkov, A., Gonzalez-Freire, M., Tharakan, R., Shardell, M., Moaddel, R., Semba, R.D., Chia, C.W., Gorospe, M., Sen, R., and Ferrucci, L. (2019). Discovery proteomics in aging human skeletal muscle finds change in spliceosome, immunity, proteostasis and mitochondria. Elife *8*, e49874.

Verdin, E. (2015). NAD+ in aging, metabolism, and neurodegeneration. Science *350*, 1208–1213.

Vogel, S.N., Henricson, B.E., and Neta, R. (1991). Roles of interleukin-1 and tumor necrosis factor in lipopolysaccharide-induced hypoglycemia. Infect. Immun. *59*, 2494–2498.

Wang, G., Han, T., Nijhawan, D., Theodoropoulos, P., Naidoo, J., Yadavalli, S., Mirzaei, H., Pieper, A.A., Ready, J.M., and McKnight, S.L. (2014). P7C3 neuroprotective chemicals function by activating the rate-limiting enzyme in NAD salvage. Cell *158*, 1324–1334.

Wang, L., Xing, X., Chen, L., Yang, L., Su, X., Rabitz, H., Lu, W., and Rabinowitz, J.D. (2019). Peak annotation and verification engine for untargeted LC-MS metabolomics. Anal. Chem. *91*, 1838–1846.

Wei, X., Jia, R., Wang, G., Hong, S., Song, L., Sun, B., Chen, K., Wang, N., Wang, Q., Luo, X., and Yan, J. (2020). Depot-specific regulation of NAD+/SIRTs metabolism identified in adipose tissue of mice in response to high-fat diet feeding or calorie restriction. J. Nutr. Biochem. *80*, 108377.

Wu, X., H.F., Zeng, J., Han, L., Qiu, D., Wang, H., Ge, J., Ying, X., and Wang, Q. (2019). NMNAT2-mediated NAD+ generation is essential for quality control of aged oocytes. Aging Cell *8*, e12955.

Yang, H., Yang, T., Baur, J.A., Perez, E., Matsui, T., Carmona, J.J., Lamming, D.W., Souza-Pinto, N.C., Bohr, V.A., Rosenzweig, A., et al. (2007). Nutrient-sensitive mitochondrial NAD+ levels dictate cell survival. Cell *130*, 1095–1107.

Yang, Y., and Sauve, A.A. (2016). NAD+ metabolism: bioenergetics, signaling and manipulation for therapy. Biochim. Biophys. Acta *1864*, 1787–1800.

Yoshida, M., Satoh, A., Lin, J.B., Mills, K.F., Sasaki, Y., Rensing, N., Wong, M., Apte, R.S., and Imai, S.I. (2019). Extracellular vesicle-contained eNAMPT delays aging and extends lifespan in mice. Cell Metab. *30*, 329–342.e5.

Yoshino, J., Baur, J.A., and Imai, S.I. (2018). NAD(+) intermediates: the biology and therapeutic potential of NMN and NR. Cell Metab. *27*, 513–528.

Zhang, H., Ryu, D., Wu, Y., Gariani, K., Wang, X., Luan, P., D'Amico, D., Ropelle, E.R., Lutolf, M.P., Aebersold, R., et al. (2016). NAD+ repletion improves mitochondrial and stem cell function and enhances life span in mice. Science *352*, 1436–1443.

Zhu, X., S.W., Wang, Y., Jaiswal, A., Ju, Z., and Sheng, Q. (2017). Nicotinamide adenine dinucleotide replenishment rescues colon degeneration in aged mice. Signal Transduct. Target. Ther. *7*, 17017.

Zhu, X.H., Lu, M., Lee, B.Y., Ugurbil, K., and Chen, W. (2015). In vivo NAD assay reveals the intracellular NAD contents and redox state in healthy human brain and their age dependences. Proc. Natl. Acad. Sci. USA *112*, 2876–2881.

Please cite this article in press as: McReynolds et al., NAD+ flux is maintained in aged mice despite lower tissue concentrations, Cell Systems (2021), https://doi.org/10.1016/j.cels.2021.09.001

STAR★METHODS

KEY RESOURCES TABLE

REAGENT OR RESOURCE	SOURCE	IDENTIFIER
Chemicals		
FK866	Selleck Chemicals	Catalog No. S2799; CAS No. 658084-64-1
LPS (E. coli 055:B5, L-2880)	Sigma–Aldrich	L2880; CAS No. 93572-42-0
[U-^{13}C]TRP	Cambridge Isotope Laboratories	Cat. #CLM-4290-H-PK
[2,4,5,6-^{2}H]NAM	Cambridge Isotope Laboratories	Cat. #DLM-6883-PK; CAS 347841-88-7
Experimental Models: Organisms/Strains		
C57BL/6J.Nia (Catheter implanted in the right jugular vein)	National Institute on Aging Rodent Colony	N/A
40% caloric restricted C57BL/6J.Nia mice (Catheter implanted in the right jugular vein)	National Institute on Aging Rodent Colony	N/A
Software and Algorithms		
MAVEN software	http://genomics-pubs.princeton.edu/mzroll/index.php	N/A
Metabolic flux analysis	https://github.com/XiaoyangSu/NAD-fluxes	N/A
Metabolomics and isotope tracing raw dataset	https://massive.ucsd.edu/ProteoSAFE/dataset.jsp?accession=MSV000087933	MSV000087933

RESOURCE AVAILABILITY

Lead contact

Further information and requests for resources and reagents should be directed to and will be fulfilled by the Lead Contacts, Joseph Baur (baur@pennmedicine.upenn.edu) and Joshua Rabinowitz (joshr@princeton.edu).

Materials availability

This study did not generate new materials.

Data and code availability

- All metabolomics and isotope tracing data reported have been deposited at MassIVE (Mass Spectrometry Interactive Virtual Environment) and are publicly available as of the date of publication. Accession numbers are listed in the key resources table.
- The code for metabolic flux analysis of *in vivo* NAD metabolism is available at https://github.com/XiaoyangSu/NAD-fluxes.
- Any additional information required to reanalyze the data reported in this paper is available from the lead contacts upon request.

EXPERIMENTAL MODEL AND SUBJECT DETAILS

Animal use and care

All animal procedures were conducted at the University of Pennsylvania and approved by the Institutional Animal Care and Use Committee. Male C57BL/6J.Nia mice were obtained from the National Institute on Aging Rodent Colony at 3 months (young) and 25 months (old) and acclimatized in the animal facility with *ad libitum* access to laboratory diet 5010 and water on 12h light: dark cycle (7AM- 7PM) for 2-4 weeks. Catheter was surgically implanted in the right jugular vein of the mouse and infusion with isotopically labeled tracer carried out mostly within a week. Single-housed aged ad libitum fed and 40% caloric restricted C57BL/6J.Nia mice (21-23 mo) were procured from National Institute on Aging Rodent Colony and maintained on NIH-31 and NIH-31 fortified diet, respectively for two months prior to use. CR mice were fed a 3g pellet everyday between 8-10 am. Three month old C57BL/6J.Nia mice were single-housed and fed *ad libitum* with NIH-31 for one month prior to catheterization and used as young controls for CR mice.

METHOD DETAILS

Intravenous infusion of mice

Isotope labeled NAD precursors, [2,4,5,6-^{2}H]-NAM and [U-^{13}C]-Trp (Cambridge Isotope Laboratories, Tewksbury, MA), were infused in young and aged mice for 2-25 hours to achieve steady state NAD labeling from labeled precursors in different tissues (Liu et al.,

Please cite this article in press as: McReynolds et al., NAD+ flux is maintained in aged mice despite lower tissue concentrations, Cell Systems (2021), https://doi.org/10.1016/j.cels.2021.09.001

2018). A tether and swivel system (Instech Laboratories, Plymouth Meeting, PA) was used for infusions to provide free movement of mouse in the cage with bedding materials and access to food and hydrogel (Clear H2O, Portland, ME). Infusion conditions in the various experiments are as follows: (1) 50mM [U-^{13}C]-Trp dissolved in saline was infused for 15hr based on their lean mass (1μL per 20 g lean mass per minute) starting at ZT0-2 (2) 4mM [2,4,5,6-^{2}H]-NAM in saline was infused for 2hr, 8hr or 24hr at a constant rate of 1μL per 20 g body weight per minute starting at ZT14-17 (3) Mice in the CR experiment were infused with 4mM [2,4,5,6-^{2}H]-NAM for 12hr starting from ZT23-ZT1 at a constant rate of 1μL per 20 g lean mass (4) In the FK866 experiment, mice were injected with vehicle (45% Propylene glycol, 5% Tween 80, 50% water) or 50 mg/kg FK866 (Selleck Chemicals, Houston, Tx) once every 8hr from ZT14, and infused after 1hr with 4mM [2,4,5,6-^{2}H]-NAM at 1μL per 20 g body weight per minute rate for 23hr (5) for LPS treatment, mice were injected with saline or 6 mg/kg LPS (E. coli 055:B5, L-2880; Sigma–Aldrich, St. Louis, MO) and immediately subjected to 4mM [2,4,5,6-^{2}H]-NAM intravenous infusion at 1μL per 20 g body weight per minute rate for 8h.

Blood samples (~20uL) were collected via tail bleeding using microvette blood collection tubes (Sarstedt, Cat. # 16.440.100) and centrifuged at 16,000 g for 15 minutes at 4°C to isolate serum. At the end of the infusion period, mice were euthanized by cervical dislocation and tissues were quickly dissected and clamped in liquid nitrogen. Serum and tissues samples were kept at -80°C before metabolite extraction for mass spectrometry analysis. Blood urea nitrogen measurements were performed on serum samples collected before and after 8h LPS treatment (Medtest Dx, Cat. # B7552).

Metabolite extraction from serum and tissues

Serum was thawed on ice before adding either -80°C 100% methanol or -80°C 80:20 methanol:water with a volume of 13.5μL solvent per 1μL serum, vortexed, incubated on dry ice for 10 minutes, and centrifuged at 16,000 g for 20 minutes, with the supernatant used for LC-MS analysis. Frozen tissues were weighed, ground with a liquid nitrogen in a cryomill (Retsch) at 25 Hz for 45 seconds, before extracting tissues with 40:40:20 acetonitrile:methanol:water (Figures 1, 2, 3, 4, and 5) or 40:40:20 acetonitrile:methanol:water supplemented with 0.1M formic acid (Figures 6 and 7) with a volume of 40μL solvent per 1mg of tissue, vortexed for 15 seconds, and incubated on ice for 10 minutes. We began adding formic acid to later experiments based on the demonstration that it improves the recovery of reduced nucleotides, and these samples were neutralized with 15% NH4HCO3 as described (Lu et al., 2018). Tissue samples were then centrifuged at 16,000 g for 30 minutes. The tissue supernatants were transferred to new Eppendorf tubes and then centrifuged again at 16,000 g for 25 minutes to remove and residual debris before analysis.

Eyes were enucleated and transferred to a 35 mm petri dish containing sterile PBS. The posterior half of the eye was trimmed of fat, muscle, and separated from the optic nerve. The anterior half of the eye, including the lens, was removed, and the retina was gently separated from the RPE using fine forceps. The separated retina and eye cup (RPE, choroid, and sclera complex) were dabbed with Kim wipes to remove moisture and snap frozen in microcentrifuge tubes in liquid nitrogen, then stored at -80 °C. The retina and eye cup were ground with a liquid nitrogen in a cryomill (Retsch) at 25 Hz for 45 seconds, before extracting with -80°C 80:20 methanol:water with a volume of 40μL solvent per mg retina or eye cup, vortexed, incubated on dry ice for 10 minutes, and centrifuged at 16,000 g for 20 minutes, with the supernatant used for LC-MS analysis.

NAD measurement by enzymatic cycling assay

Tissue samples were extracted with 0.6M perchloric acid using a TissueLyzer (Qiagen). NAD content was measured by an enzymatic cycling assay in a 96-well format as described previously(Frederick et al., 2015). Briefly, 5 μl of NAD standards or diluted tissue extracts was combined with 95 μl of cycling mixture (2% ethanol, 100 μg/ml alcohol dehydrogenase, 10 μg/ml diaphorase, 20 μM resazurin, 10 μM flavin mononucleotide, 10 mM nicotinamide, 0.1% BSA in 100 mm phosphate buffer, pH 8.0). Resorufin accumulation was measured over the period of 30min at room temperature by fluorescence excitation at 544 nm and emission at 590 nm.

Immune cell sorting and metabolite extraction

Metabolites were extracted from sorted immune cell subpopulations from spleen. Briefly, half of the spleen was smashed and passed through a 70μm strainer. After a cold PBS (Corning #21-031-CV) wash and centrifugation, pellets were resuspended in 1.5ml of Ammonium-Chloride-Potassium buffer (Gibco #A10492-01) for 3min at room temperature. Lysis was blocked by dilution in 30ml of cold PBS. Single cell suspensions were stained with 1μl of each antibody (CD45-APC (30-F11), CD11b PeCy7 (M1/70), CD3 BV510 (17A2) B220 Pe (RA3-6B2) from EBiosciences) for 1.10^6 cells in 100μl of PBS at 4°C protected from light for 30min. After staining, cells were washed once and resuspended in PBS containing 1% of deactivated FBS (Thermofisher sci. #10082147). Sorting was performed on a BD FACSAria Fusion cell sorter. Sorted cells were centrifuged and resuspended in 40:40:20 acetonitrile:methanol:water supplemented with 0.1M formic acid and neutralized with 15% NH4HCO3.

Extraction of Mitochondrial Metabolites

Mitochondria was isolated from fresh tissues as reported previously (Frederick et al., 2015). Tissue samples were minced in ice-cold mitochondrial isolation buffer (210mM Mannitol, 70mM Sucrose, 10mM HEPES, 1mM EGTA, pH 7.4 with 0.25% fatty acid free bovine serum albumin), and homogenized with Potter Elvehjem homogenizer for 6-10 passes at 150 rpm. The homogenate was centrifuged at 750g for 5 min, and pellet was washed twice at 5000g for 20 min at 4°C. Isolated mitochondria was resuspended in mitochondrial isolation buffer to measure protein concentration and citrate synthase assay. Pelleted mitochondria was extracted using 40:40:20 acetonitrile:methanol:water with 0.1M formic acid. The extract was neutralized with 15% NH4HCO3.

Please cite this article in press as: McReynolds et al., NAD+ flux is maintained in aged mice despite lower tissue concentrations, Cell Systems (2021), https://doi.org/10.1016/j.cels.2021.09.001

Metabolite measurement

Extracts were analyzed within 24 hours by liquid chromatography coupled to a mass spectrometer (LC-MS). The LC–MS method involved hydrophilic interaction chromatography (HILIC) coupled to the Q Exactive PLUS mass spectrometer (Thermo Scientific) (Wang et al., 2019). The LC separation was performed on a XBridge BEH Amide column (150 mm 3 2.1 mm, 2.5 mm particle size, Waters, Milford, MA). Solvent A is 95%: 5% H2O: acetonitrile with 20 mM ammonium bicarbonate, and solvent B is acetonitrile. The gradient was 0 min, 85% B; 2 min, 85% B; 3 min, 80% B; 5 min, 80% B; 6 min, 75% B; 7 min, 75% B; 8 min, 70% B; 9 min, 70% B; 10 min, 50% B; 12 min, 50% B; 13 min, 25% B; 16 min, 25% B; 18 min, 0% B; 23 min, 0% B; 24 min, 85% B; 30 min, 85% B. Other LC parameters are: flow rate 150 ml/min, column temperature 25°C, injection volume 10 μL and autosampler temperature was 5°C. The mass spectrometer was operated in both negative and positive ion mode for the detection of metabolites. Other MS parameters are: resolution of 140,000 at m/z 200, automatic gain control (AGC) target at 3e6, maximum injection time of 30 ms and scan range of m/z 75-1000. Raw LC/MS data were converted to mzXML format using the command line "msconvert" utility (Adusumilli and Mallick, 2017). Data were analyzed via the MAVEN software, and all isotope labeling patterns were corrected for natural ^{13}C abundance using AccuCor (Su et al., 2017).

QUANTIFICATION AND STATISTICAL ANALYSIS

Quantification of NAD+ Fluxes *In Vivo*

We infused [U-$^{13}C_{11}$] Trp and [2,4,5,6-$^{2}H_4$] NAM separately to mice to determine fluxes. [U-$^{13}C_{11}$] Trp (Trp_{11}) resulted in NAD_6 (NAD M+6 with all carbons on the nicotinamide part labeled) and then $NAM_{Tissue,6}$. $NAM_{Tissue,6}$ was then exchanged between tissues and circulation ($NAM_{Serum,6}$) before being taken by tissues to make NAD. NAD_3 was made directly from NAM_4 (one deuteron of NAM_4 becomes the redox-active deuteron of NAD and thus is quickly lost). Breakdown of NAD_3 yields NAM_3.

In each organ, as shown in Figure 3, 4 NAD metabolic fluxes are calculated assuming metabolic steady state in each tissue: f_1 is NAD *de novo* synthesis flux from tryptophan, f_2 is the flux of NAM being taken up from serum, f_3 is NAD synthesis flux from tissue nicotinamide (NAM). At metabolic steady state, the NAD and nicotinamide concentrations in tissue stay constant. Therefore, the mass balance suggests the corresponding breakdown (NAD → NAM) and excretion (tissue NAM → circulation) fluxes are fully determined by the production fluxes above, and thus are not included as separate variables in the model. The following set of differential equations are used to calculate the tissue NAD and NAM labeling patterns at each time point.

$$\begin{cases}
\frac{dNAD_0}{dt} = \frac{[f_1(Trp_0 - NAD_0) + f_3(NAM_{Tissue0} - NAD_0)]}{c_{NAD}} \\
\frac{dNAD_3}{dt} = \frac{[f_1(-NAD_3) + f_3(NAM_{Tissue3} + NAM_{Tissue4} - NAD_3)]}{c_{NAD}} \\
\frac{dNAD_6}{dt} = \frac{[f_1(Trp_{11} - NAD_6) + f_3(NAM_{Tissue6} - NAD_6)]}{c_{NAD}} \\
\frac{dNAM_{Tissue0}}{dt} = \frac{[(f_1 + f_3)(NAD_0 - NAM_{Tissue0}) + f_2(NAM_{Serum0} - NAM_{Tissue0})]}{c_{NAM}} \\
\frac{dNAM_{Tissue3}}{dt} = \frac{[(f_1 + f_3)(NAD_3 - NAM_{Tissue3}) + f_2(NAM_{Serum3} - NAM_{Tissue3})]}{c_{NAM}} \\
\frac{dNAM_{Tissue4}}{dt} = \frac{[(f_1 + f_3)(-NAM_{Tissue4}) + f_2(NAM_{Serum4} - NAM_{Tissue4})]}{c_{NAM}} \\
\frac{dNAM_{Tissue6}}{dt} = \frac{[(f_1 + f_3)(NAD_6 - NAM_{Tissue6}) + f_2(NAM_{Serum6} - NAM_{Tissue6})]}{c_{NAM}}
\end{cases}$$

(Figure 3)

In the equations, NAD_i represent the labeling fraction of mass isotopomer M+i of tissue NAD. $NAM_{Tissue\ i}$ and $NAM_{Serum\ i}$ represent the labeling fraction of tissue NAM and serum NAM M+i, respectively. Trp_{11} represents the labeling fraction of serum tryptophan. c_{NAD} and c_{NAM} are tissue concentrations of NAD(H) and NAM, respectively (in nmol/gram tissue weight).

Tryptophan reached steady state in serum within 30 min, therefore Trp_{11} was treated as constants (59% and 60% in young and old animals, respectively). Serum NAM labeling changes as a function of time. In our differential equations, we did not simulate the serum NAM labeling. Instead, the serum NAM labeling was measured experimentally at a few time points, and the empirical labeling kinetics was obtained through polynomial interpolation. At t=0, NAD_{M+0}, NAM_{M+0} are 1, while all other fractions are 0. For any given set of the three fluxes, the dynamic labeling patterns can be calculated from the differential equations. The calculated values were then compared to the measured labeling patterns of tissue NAM and NAD (2 h, 8 h, 24 h during [2,4,5,6-^{2}H] NAM infusion, 15 h after [U-^{13}C] Trp infusion). The tissue concentration of NAM and NAD were also measured. The best estimated flux set is achieved by

Please cite this article in press as: McReynolds et al., NAD^+ flux is maintained in aged mice despite lower tissue concentrations, Cell Systems (2021), https://doi.org/10.1016/j.cels.2021.09.001

minimizing the deviation between the calculated labeling patterns and the measured ones. The deviation in each labeled fraction is weighted by the reciprocal of the standard deviation of the replicate experimental labeling measurements. The numerical simulation of the differential equations was performed in R with the deSolve package and the optimization was performed with DEoptim package. 95% confidence intervals of the NAD turnover rates were estimated by chi-square test (cutoff $\chi^2_{0.05}(df=1)=3.84$) (Antoniewicz et al., 2006).

Statistical analysis

Data are displayed as mean ± SEM. In figures, asterisks denote statistical significance as calculated by a two-tailed unpaired Student's t-test or 2-way ANOVA (§, $p < 0.1$, *, $p < 0.05$; **, $p < 0.01$; ***, $p<0.001$). This test is appropriate for determining whether the means of two populations are equal. Data were not tested for the assumptions of normality and equal variance across groups. Exponential curve fitting was used to test whether data followed an exponential decay pattern. Statistical parameters are reported in the Figures and Figure Legends. $P<0.05$ was considered statistically significant. N represents the number of replicates.